Building and Environment 225 (2022) 109648

Contents lists available at ScienceDirect

Building and Environment

journal homepage: www.elsevier.com/locate/buildenv

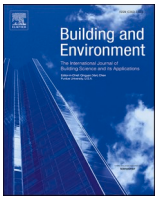

Parametric study of a novel combination of solar chimney and radiative cooling cavity for natural ventilation enhancement in residential buildings

Suhendri Suhendri, Mingke Hu [*,1], Yuehong Su [1], Jo Darkwa, Saffa Riffat

Department of Architecture and Built Environment, University of Nottingham, Nottingham, NG7 2RD, UK

ARTICLE INFO

Keywords:
Radiative cooling
Solar chimney
Natural ventilation
Passive cooling
Parametric study

ABSTRACT

The application of radiative cooling (RC) is expanding to a diverse research field, with some current studies trying to apply RC for natural ventilation. One proposed strategy is to use RC for the enhancement of solar chimney (SC) ventilation, and this strategy has been proven in a dry temperate climate. However, geographical locations and other design parameters may affect the performance of this natural ventilation strategy, and the conditions in which SC-RC ventilation performs best need to be investigated. This parametric study examines the performance of a novel SC-RC ventilation with six different parameters. The six parameters are the RC emitter's convection cover, building's thermal mass, RC cavity gap, internal heat gain, climate, and fan usage. Transient 2D computational fluid dynamics (CFD) simulations with Ansys Fluent were conducted to analyse the SC-RC ventilation's optimal design and working conditions. A convection cover on the RC emitter, a thermal mass wall material, a smaller RC gap, and a relatively low internal heat gain help the SC-RC achieve a cooler room and higher ventilation flow rate. Overall, the novel SC-RC ventilation performance is better than a conventional SC, except in humid climates. In dry climates, the SC-RC has the potential to create a maximum 2 °C temperature reduction, with a daily average room temperature of 0.56 °C lower than ambient. This cooling performance of the passive SC-RC ventilation is better than the fan-assisted SC-RC. Also, the SC-RC can achieve a daily average of 2.1 ACH, which is 0.4 ACH more than the conventional SC.

1. Introduction

Radiative sky cooling (or radiative cooling) research has been very productive recently. Radiative cooling (RC) emitters exploit the cold outer space as a heat sink, with the atmosphere as the window. In a clear sky, the atmosphere has a high transmissivity for radiation at 8–13 μm wavelength, known as the atmospheric window band. Favourably, the emissive power of an RC emitter also peaks in this atmospheric window band so that it is possible for the emitter to continuously radiate a considerable amount of heat to outer space [1,2]. These RC emitters may easily achieve a sub-ambient temperature at night. However, in the daytime, the emitters must reflect almost all the solar radiations to still get the intended cooling effect. Research on affordable and readily available RC materials with high solar reflectivity and high thermal emissivity in the atmospheric window band for 24-h cooling is among the objectives of current RC research.

The possible application of RC in various sectors has also been a theme in RC research. In the building sector, RC has been used in both passive and active cooling strategies [3,4]. For instance, recent studies tried to use RC to passively cool a building by applying an RC material or coating on the roof of a building to reduce heat gains to the structure [5–7]. One example of RC used in an active system for buildings is an RC-enhanced solar absorption chiller [8]. This RC-enhanced chiller is significantly more efficient than a conventional chiller [8]. Besides its use for cooling, current research also exploits RC to enhance natural ventilation in buildings [9,10]. A colder-than-air RC emitter cools the adjacent air, making it denser than the ambient air, and thus the air sinks. Because this downward flow carries a lower temperature air than the surrounding, it also creates a cooling effect. This similar phenomenon is employed in ceiling radiant cooling systems to promote thermal comfort in a room [11–13]. A study from Li et al. [14] has even proven that this gravity-driven flow is effective for cooling a dual-cavity window to reduce heat gain to the building.

Architects may have realised the ventilation and cooling benefit of this RC-induced natural convection flow at night. The strategy is known as nocturnal cooling and has been proposed in many passive design strategies [1,15]. However, the potential for this RC ventilation for the

* Corresponding author.
E-mail address: mingke.hu@nottingham.ac.uk (M. Hu).
[1] The two authors have the same contribution to this study.

https://doi.org/10.1016/j.buildenv.2022.109648
Received 20 July 2022; Received in revised form 5 September 2022; Accepted 27 September 2022
Available online 4 October 2022

Nomenclature

C	specific heat capacity ($J{\cdot}kg^{-1}{\cdot}K^{-1}$)
E	total energy (J)
F	inclination angle factor
$\vec{F}$	external body forces (N)
g	gravitational acceleration ($m{\cdot}s^{-2}$)
H	solar irradiance ($W{\cdot}m^{-2}$)
h	heat transfer coefficient ($W{\cdot}m^{-2}{\cdot}K^{-1}$)
k_{eff}	effective thermal conductivity ($W{\cdot}m^{-1}{\cdot}K^{-1}$)
p	static pressure (Pa)
P_v	water vapor pressure (mbar)
q	heat flux ($W{\cdot}m^{-2}$)
T	temperature (°C)
t	time (s)
U	thermal transmittance ($W{\cdot}m^{-2}{\cdot}K^{-1}$)
v	air velocity ($m{\cdot}s^{-1}$)

Greek letters

α	thermal expansion coefficient of air
ΔT	temperature difference (°C)
ε	emissivity
ρ	density ($kg{\cdot}m^{-3}$)
σ	Stefan-Boltzmann constant (5.67×10^{-8} W m^{-2} K^{-4})
τ	transmissivity
τ	stress tensor

Abbreviations

ACH	air change per hour
CFD	computational fluid dynamics
DO	discrete ordinates
PE	polyethylene
PT	photothermal
RC	radiative cooling
RMSD	root mean square deviation
SC	solar chimney
TMY	typical meteorological year
UDF	user-defined function
NV	naturally ventilated

Subscript

bs	absorber
amb	ambient
cond	conduction
conv	convection
dp	dew point
emit	RC emitter
env	building envelope
ext	exterior side
ind	indoor
int	interior side
rad	radiation
sol	solar
surf	building's surface

entire day is still under-studied. A high-power passive daytime RC, with the current maximum achieved in an experiment around 150 W/m^2 [16], is still much lower than the cooling power needed to drive the intended flow during the daytime. Even the heat gain from solar fenestration in a 3 m by 4 m room could be five times higher than the RC cooling power during the day [17]. This limitation causes the use of RC as the main provider of natural ventilation to buildings to be impractical.

To overcome the previously mentioned issues, this study proposes a novel use of RC by combining it with solar chimney (SC) ventilation. SC is a well-known natural ventilation strategy employing a solar absorber to heat the air inside a chimney. The lighter hot air flows upward, creating a condition for the ventilation flow inside the building. Resorting to CFD simulation, many studies have investigated ways to improve SC ventilation performance by maintaining its effectivity at night-time, increasing its ventilation rate, and enhancing its cooling performance. To extend the working time of SC to the night, researchers commonly incorporated a phase change material (PCM) into the SC absorber [18–20]. Amori and Mohammed [18] found that the PCM successfully extends the SC ventilation to night-time. Tiji et al. [19] further improved the performance of SC-PCM by employing a finned absorber. They concluded that the flow rate of the finned absorber SC-PCM increased by 40%.

Various strategies have been proposed for ventilation rate and cooling performance improvements, and many of them are by combining SC with other natural ventilation or passive cooling techniques [21,22]. For instance, Rabani et al. [18] showed an improvement in ventilation rate and daily cooling efficiency by combining SC with a Trombe wall and water spray. Similarly, Moosavi et al. [22] used water spray as the pre-cooling mechanism of the inlet air but used a wind catcher to increase the ventilation rate. They reported improvements in the ventilation and cooling performance of the SC ventilation. Another way of pre-cooling the inlet air of the SC ventilation is through an earth-to-air heat exchanger (EAHE) [23–25]. Long et al. [25] conducted a parametric study on the SC-EAHE strategy and identified the system's optimal design and environmental conditions.

In the SC-RC ventilation strategy proposed in this study, an RC cavity is devised to improve daytime ventilation and cooling performance. The RC cavity is also the primary driver of ventilation flow at night. A parametric study is conducted to find the optimal design parameters and comprehensively understand the potential of SC-RC ventilation in different conditions. Similar to most of the studies mentioned above on SC ventilation, this study also employs CFD to investigate the performance of the SC-RC ventilation in various working conditions and parameters. The CFD simulation is conducted in ANSYS Fluent 2021 [26] using dynamic analyses to reasonably model the dynamic response of the ventilation strategy to those different conditions or design parameters.

2. System design and parameters

The schematic of the proposed SC-RC ventilation is shown in Fig. 1. The SC is placed on the sun-facing side of a roof, combined with an RC cavity on the opposite side. During the daytime, the SC is heated by solar radiation to generate a buoyancy effect that draws air from the room and the RC cavity. While the air flows through the RC cavity, it gets cooled by the RC surface and provides chilled air for the room. An insulation material encloses all the inner ceiling channel walls to minimise conduction heat loss from the absorber, SC, and RC cavity to the attic space.

In addition to that, two groups of parameters have been identified to affect SC and RC performance. The first group is parameters related to the environment, such as solar irradiance and clear sky index. Those two parameters affect the RC emitter's ability to be in a sub-ambient temperature. However, if SC needs higher solar radiation, the RC emitter is the opposite. Other parameters, such as ambient temperature, humidity, and wind speed, are also reported to have a significant influence on the performance of RC [27–29], although their effect is not so straightforward for SC.

The second group is parameters associated with the SC and RC systems design. For example, the sky view factor, indicated by inclination

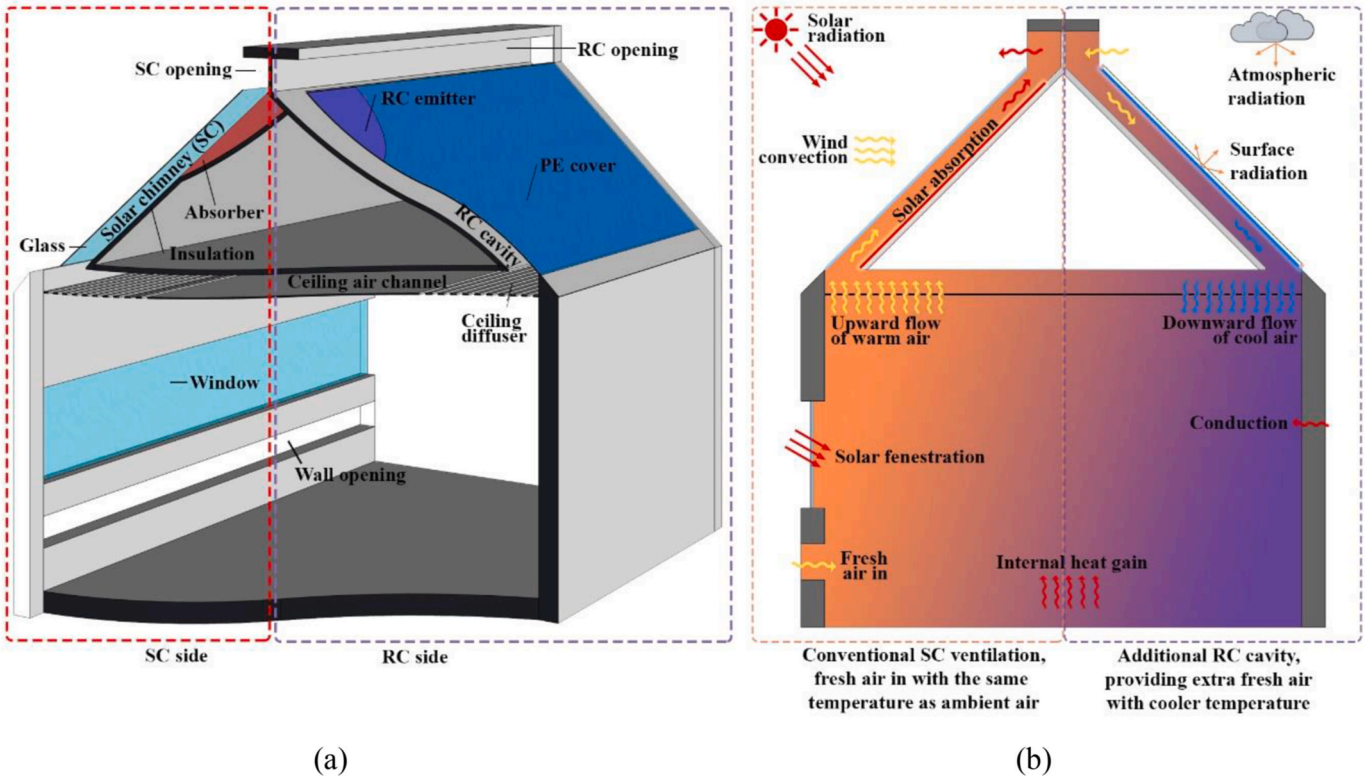

Fig. 1. (a) Schematic diagram of roof solar chimney combined with radiative cooling cavity applied in a building and (b) cross-sectional diagram of the transfer phenomena in the building.

angle, affect both SC and RC performance. The optimal inclination angle for SC is latitude-related [30]. In contrast, the optimal angle for RC is horizontal at night [31] or when tilted at a certain inclination angle to the opposite direction of the sun in daytime [32,33]. Chimney length and width are also important parameters in SC design [34–36], although different studies reported different optimal values. It may be said that the preferred SC length is 1.5 m [34], but it is common for an SC to have the same length as a building's wall or roof. The chimney width is more flexible, ranging from 5 cm to 30 cm, but a 20 cm chimney gap is considered the best width [34]. For RC emitter, it is also worth mentioning that RC's most important parameters are the spectral emissivity of the emitter [37,38]. To achieve daytime sub-ambient RC, the emitter must show extremely low absorptivity in the solar spectrum and very high emissivity in the atmospheric window band [39,40]. Also, to reduce the convective heat gain and improve RC power, a convection cover (usually polyethylene (PE) film) that is transparent in that specific band is commonly employed [41].

There are other design-related parameters, but more to the building design rather than the SC or RC system design. One of the parameters is the building's thermal mass, which may directly or indirectly strengthen or weaken the ventilation rate of a buoyancy-driven ventilation strategy [42]. Thermal mass materials are commonly used as wall materials and cover a substantial part of a building. Hence, the thermal storage capacity of the thermal mass regulates temperature changes in a room and affects the air movement to, from, and inside the room. If the thermal mass wall mainly deals with the external heat gains of the building, the building's internal heat gains also matter when using buoyancy-driven ventilation because it also affects the indoor air temperature [43]. In some SC research, a fan is also considered to assist the natural ventilation performance when the condition is not desirable [44–46].

3. Methodology

3.1. Case study building

A hypothetical building with a cross-sectional width of 4 m, a length of 6 m, and a ceiling height of 2.8 m was designed to be the case study building. The building has a gable roof with a 45° inclination angle, with the roof sides facing south and north. On the south-facing (sun-facing in the northern hemisphere) roof, an SC is placed with an air-channel gap of 20 cm and a 30 cm opening at the top as the outlet (SC opening). An RC cavity is placed on the opposite north-facing roof with a default gap of 20 cm. This RC cavity gap is then varied according to values in the study of the effect of the RC cavity gap on the SC-RC performance. The RC cavity has its opening (RC opening) as the inlet at the top of the cavity. On the ceiling, the RC cavity and SC air channels are merged into a ceiling air channel, with diffuser-like openings on the SC and RC sides. These openings are joined by another opening at the bottom side of the SC-side wall (wall opening) that functions as the original inlet opening of the SC ventilation. The reference case to be compared is the SC ventilation, where the RC cavity is closed. Fig. 2 helps to illustrate the geometry and dimension of the case study building.

The default location for the parametric studies was Valencia (39.5°N, 0.4°W), which according to Koppen-Geiger climatic classification, is classified as a warm temperate, dry, and hot summer climate (Csa) [47]. Hence, the climate is considered suitable for our SC-RC ventilation's cooling and ventilation purposes. The hottest day in Valencia, on the 29th of July, based on typical meteorological data (TMY) [48], was chosen for the simulation. The ambient temperature, wind speed, and global solar irradiance of Valencia on the hottest day are shown in Fig. 3.

Further, the construction materials of the case study were based on the common construction materials for buildings. Brick was used for wall material with 20 cm of thickness and ceramic, timber, and roof tile for floor, ceiling, and roof materials, respectively [49]. Additionally, the absorber and emitter in the SC and RC cavity used aluminium with a

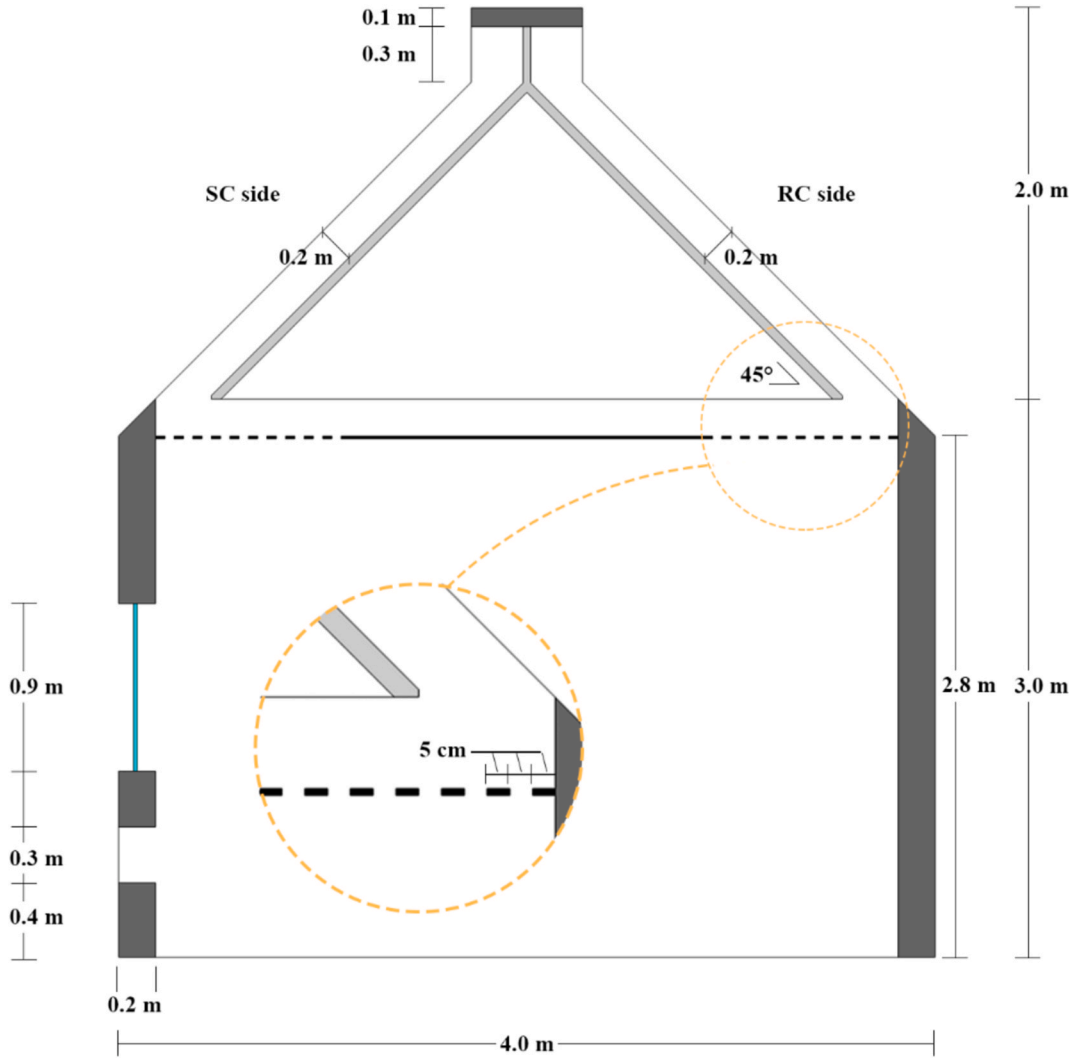

Fig. 2. Geometry and dimension of the case study building.

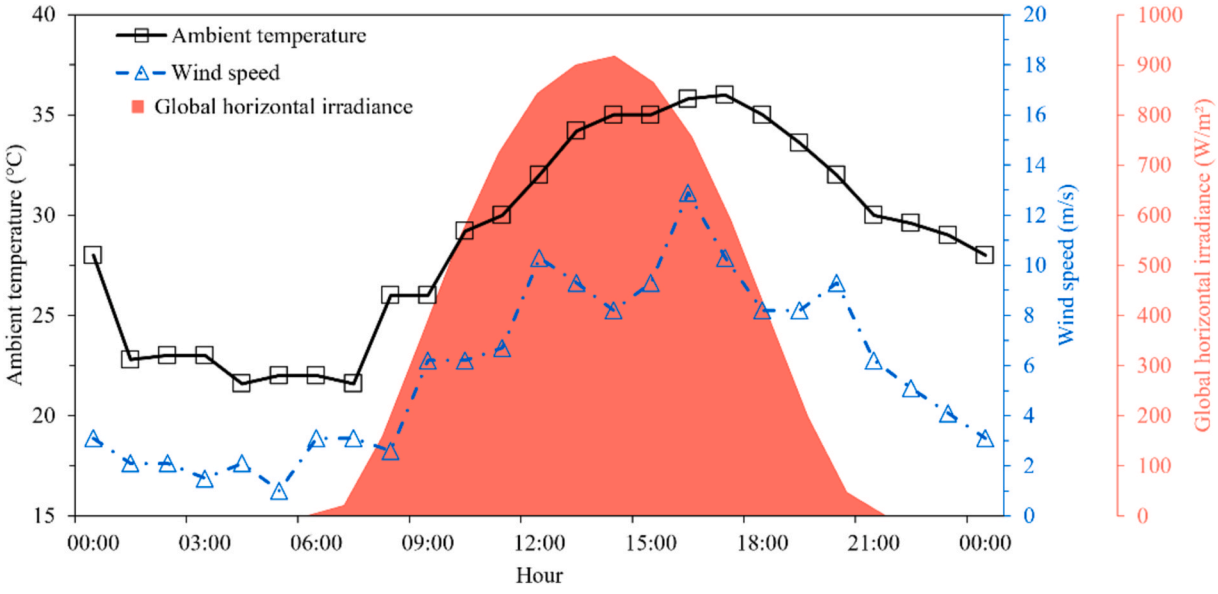

Fig. 3. The ambient temperature, wind speed, and global solar irradiance on the 29th of July taken from the TMY of Valencia [48].

thickness of 1 mm as its base, coated with a heating/cooling coating suited for its purpose. The solar absorber coating has high absorptivity in the solar radiation band (0.2–3 μm) and thermal radiation band (3–25 μm). Meanwhile, the RC emitter coating has high emissivity only in the atmospheric window band (8–13 μm) and low absorptivity in the solar spectrum (0.2–3 μm) and other thermal bands (3–8 μm and 13–25 μm). A PE film was used as the convection cover for the RC emitter. The spectral properties of the construction materials in those wavelengths and their respective thermal properties are summarised in Table 1. Except for the absorber and emitter, the emissivity for all materials was taken from the ECOSTRESS spectral library [50].

The case study building was simulated with various sets of parameters. From all the previously mentioned parameters in Section 2, all the environment-related parameters can be combined as the effect of climatic conditions or geographical location. Five warmest climates in the Köppen-Geiger climate classification were selected to be studied, namely the tropical humid (Af), steppe climate (BSh), desert climate (BWh), warm temperate and humid climate (Cfa), as well as warm temperate and dry climate (Csa) [47]. In comparing SC-RC performance in different climates, the locations were changed accordingly, but the selected day was still the hottest in the respective climate.

Other parameters relevant to the building or system design were also studied. The parameters are the RC emitter's convection cover, the building's thermal mass, the RC cavity gap, internal heat gain, and whether the SC-RC is naturally ventilated (NV) or fan-assisted. In the study of the effect of thermal mass on the ventilation flow, a comparison between a heavyweight brick wall and a 5-cm thick lightweight insulation board was made. A summary of the parameters, the variable and its base SC-RC cases, as well as the related reference SC case, are detailed in Table 2.

Table 2
Description of the studied parameters and their related base and reference cases.

Parameter	Variable SC-RC case	Base SC-RC case	Reference SC case
Convection cover	PE-covered and uncovered SC-RC with light wall material (insulation board)	PE-covered SC-RC natural ventilation, with a 20 cm thick brick wall, RC cavity gap of 20 cm, and internal heat gain of 0 W/m^2, located in Valencia (Csa)	SC-only ventilation, with a 20 cm thick brick wall, and other conditions follow the respective variable and base cases of SC-RC.
Thermal mass	SC-RC with lightweight wall material (insulation board)		
Gap	SC-RC with various RC cavity gaps: 10 cm, 15 cm, 25 cm, 30 cm		
Internal heat gain*	SC-RC with various internal heat gain: 1 W/m^2, 2 W/m^2, 3 W/m^2, 4 W/m^2		
Climate	SC-RC with various climate conditions: Af (Singapore), BSh (Lahore), BWh (Riyadh), Cfa (Shanghai)		
Fan-assisted	SC-RC with various daily average fan flow rates: 0.05 m^3/s, 0.1 m^3/s, and 0.5 m^3/s		

**The standard value for internal heat gain for a large building area is 2.*1 W/m^2 [51].

3.2. Governing equations and simulation procedure

The case study building was modelled as a 2D geometry in Ansys Fluent 2021 [26]. The simplification of the geometry in a 2D study is acceptable for an unchanging room shape [52]. Note that SC-RC ventilation is buoyancy-driven and necessitates the condition of the outdoor pressure gradient in the vertical direction to be known [52]. Therefore, the outdoor air is included in the computational domain with dimensions and conditions shown in Fig. 4 (a). The top and side boundaries of the external domain were set as a pressure field far away, and the bottom boundary of the external domain was set as the ground. The initial mesh used for the simulation was hexahedral, starting with a maximum size of 5 cm for the room (see Fig. 4 (a) and (b)) and later refining for grid-independence study until the finest size of 1 cm.

After geometry creation and meshing, the model was moved to simulation and boundary condition settings. For this step, the hourly solar irradiance and weather conditions were inputted as user-defined tabular input. Note that the solar irradiance data available in TMY is for global horizontal only. Hence, to obtain the solar irradiance on every building surface, an EnergyPlus simulation was conducted and transferred the solar irradiance data to user-defined tabular data for ANSYS Fluent. Near the end of the simulation process, one crucial step was the time step and grid independence study. Parameters checked for the time step and grid-independence study were glass, absorber, and emitter surface temperature, room air temperature, and velocity, as well as the volumetric and mass flow rate at the building openings. The discretisation settings that can give mesh and time-step independent results are used for the parametric studies.

Ansys Fluent then solves the transport equations known as the continuity, momentum, and energy equations as summarised by Equations (1)-3) [53]. In Equation (1), ρ and v represent the air density and velocity respectively, while t is time, and S_m mass addition to the system. Furthermore, in Equation (2) the letter p is the static pressure, τ is the stress tensor, ρg is the term for gravitational body force, and F is the external body forces. Also, in Equation (3) for the energy equation, the total energy of the air is represented by E, and the effective conductivity of the air is denoted by k_{eff}, and the air temperature is expressed by T. Any additional energy inputs to the system are included in S_h.

$$\frac{\partial \rho}{\partial t} + \nabla \bullet (\rho v) = S_m \tag{1}$$

$$\frac{\partial}{\partial t}(\rho v) + \nabla \bullet (\rho v v) = -\nabla p + \nabla \bullet (\bar{\bar{\tau}}) + \rho g + \vec{F} \tag{2}$$

Table 1
Thermal and spectral properties of the construction materials.

Material	Thermal properties			Absorptivity/emissivity			
	Thermal conductivity (W·m^{-1}·K^{-1})	Density (kg·m^{-3})	Specific heat capacity (J·kg^{-1}·K^{-1})	0.2–3 μm	3–8 μm	8–13 μm	13–25 μm
Brick	0.72	1920	840	0.79	0.77	0.93	0.93
Ceramic tile	0.8	1700	850	0.34	0.94	0.93	0.93
Insulation board	0.033	38	1400	0.70	0.90	0.90	0.90
Roof tile	0.8	1890	880	0.87	0.93	0.95	0.95
Timber	0.16	720	1260	0.46	0.9	0.94	0.94
Absorber	202.4	2719	871	0.95	0.95	0.95	0.95
Glass	1.38	2203	703	0.05	0.88	0.88	0.88
Emitter	202.4	2719	871	0.05	0.95	0.95	0.95
PE film	0.45	910	1900	0.05	0.05	0.05	0.05

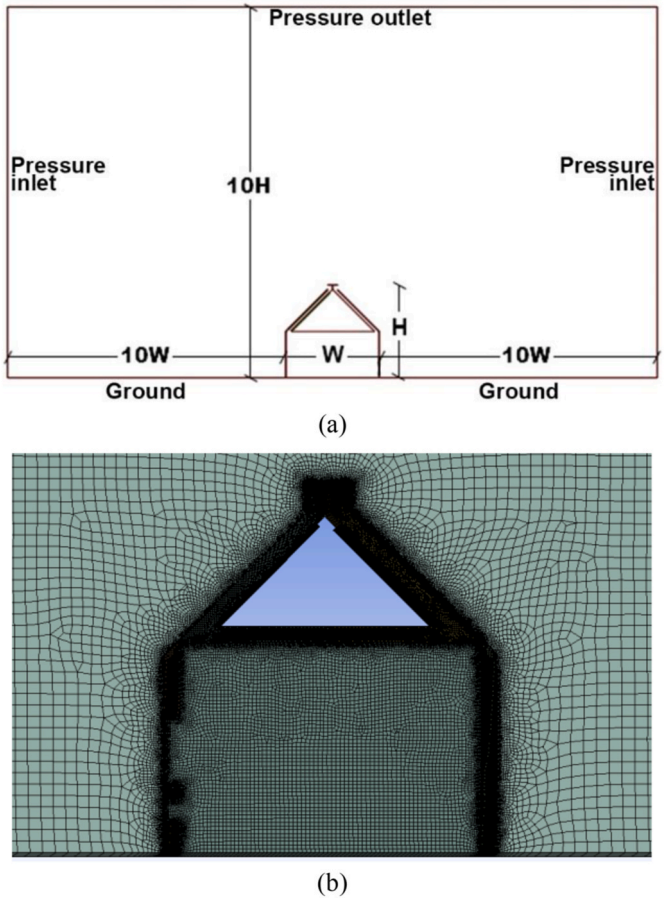

Fig. 4. (a) The computational domain of the study and (b) Initial computational grids with 5 cm maximum size in the room.

$$\frac{\partial}{\partial t}(\rho E) + \nabla \bullet (v(\rho E + p)) = \nabla \bullet (k_{\text{eff}} \nabla T + (\bar{\bar{\tau}}_{\text{eff}} \bullet v)) + S_h \tag{3}$$

Moreover, the transport equations were solved along with the Standard $k-\varepsilon$ turbulence model [54], which is considered sufficient to model a buoyancy-driven ventilation flow [55,56]. The incompressible ideal gas law is used, as the outdoor atmospheric pressure is set as constant [57]. For the radiation model, the discrete-ordinate (DO) radiation model was employed due to its capability to account for the non-grey model [57]. We also employed the commonly used SIMPLE algorithm for pressure-velocity coupling with a first-order discretisation scheme for both the convection and viscous terms and PRESTO! discretisation scheme for the pressure terms. Simulation results are judged as converged when the key parameters, namely hourly indoor air temperature and velocity and flow rate at the building openings, show stable values. Overall, the general steps for the parametric studies are illustrated in Fig. 5.

3.3. Boundary conditions

Heat transfer phenomena on the building's surface were inputted in the boundary conditions as user-defined functions (UDF). This UDF was based on the heat balance equations for the building surfaces described in the following subsections. A detailed description of the boundary conditions is available in the Appendix.

3.3.1. Heat balance of the building envelope

For this case study building, the envelope includes the SC's glass cover, the RC emitter's PE cover, the roof, and the wall (see Figs. 1 and 2). Each envelope's exterior surface receives radiation from the sun

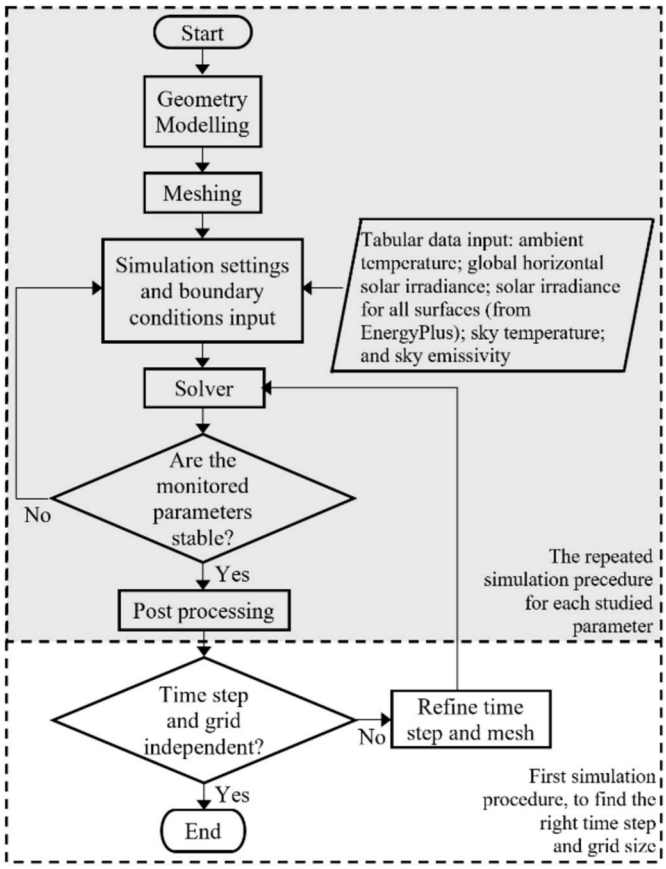

Fig. 5. Simulation logic flow diagram.

(q_{sol}), exchanges heat via radiation with the atmosphere (q_{rad}), and via convection with the outdoor ambient air ($q_{\text{conv\_ext}}$). On the interior side of the envelope, conduction heat transfer occurs across the envelop (q_{cond}), and another convection also occurs between the envelope to the interior air ($q_{\text{conv\_int}}$). The building envelope's material does not instantaneously be in a thermal equilibrium state with all those heat fluxes and may have some capacity to 'store' energy (q_{stored}). Equation (4) formulates the heat balance for the building envelopes.

$$q_{\text{sol}} + q_{\text{rad}} + q_{\text{conv\_ext}} + q_{\text{conv-int}} + q_{\text{cond}} = q_{\text{stored}} \tag{4}$$

The following equations detail each heat flux from Equation (4). In Equation (5), q_{sol} is modelled as the amount of solar radiation that is absorbed by the surface, with α_{surf} is the surface's absorptivity, and H_{surf} is the total solar irradiation received by the surface. Thermal radiation, q_{rad}, accounts for the incoming radiation from the sky ($q_{\text{rad\_sky}}$) and the outgoing radiation from the surface ($q_{\text{rad\_surf}}$), and the two terms are combined as in Equation (6). In Equation (6), ε_{sky} and $\varepsilon_{\text{surf}}$ are emissivity of the sky and the surface respectively, σ is Stefan-Boltzmann constant, T_{sky} is the sky temperature, and T_{surf} is the surface temperature. Moreover, the value of ε_{sky} and T_{sky} are calculated using an empirical

Table 3
Empirical formula used for ε_{sky} and T_{sky}

Climate condition (Location)	ε_{sky}	T_{sky}
Af (Singapore)	$\varepsilon_{\text{sky}} = 0.711 + 0.56(T_{\text{dp}}/100) + 0.73(T_{\text{dp}}/100)^2$, [58]	$T_{\text{sky}}^4 = \varepsilon_{\text{sky}} T_{\text{amb}}^4$, [59]
BSh (Lahore)	$\varepsilon_{\text{sky}} = 0.56 + 0.08P_v^{0.5}$, [60]	
BWh (Riyadh)		
Cfa (Shanghai)	$\varepsilon_{\text{sky}} = 0.754 + 0.0044T_{\text{dp}}$, [61]	
Csa (Valencia)		

considering dew point temperature (T_{dp})or water vapor pressure (P_v) of the related location as summarised in Table 3. Also, to account for the effect of envelope surface's inclination angle, the variable F_{surf} is included to Equation (6), which represents percentage of net radiation reduction with the increase of the inclination angle from the zenith angle. The value of F_{surf} is 1 for horizontal surface (top roof), and for 45° (glass, PE cover, and RC emitter surfaces) and 90° (wall surfaces) are 0.75 and 0.33, respectively [31].

$$q_{sol} = \alpha_{surf}\ H_{surf} \tag{5}$$

$$q_{rad} = q_{rad\_sky} - q_{rad\_surf} = F_{surf}\ \ \varepsilon_{sky}\ \varepsilon_{surf}\ \sigma\ (T_{sky}^4 - \ T_{surf}^4) \tag{6}$$

Furthermore, the $q_{conv-ext}$ and $q_{conv-int}$ follow the same formula with variation in the heat transfer coefficient calculation and the temperature involved in the equation, as seen in Equations (7) and (8). For the exterior side of the envelope, the heat transfer coefficient with the ambient air, h_{amb} in Equation (7), is defined using the empirical formula shown in Equation (9) [62], while the heat transfer coefficient with the ambient air, h_{int} in Equation (8), is internally calculated by Ansys Fluent. Other parameters in those equations, namely T_{amb} represents the ambient temperature, T_{ext} represents the exterior surface temperature, T_{ind_air} is the indoor air temperature adjacent to the surface, and T_{int} is the interior surface temperature. Similarly, q_{cond} in Equation detailed in (10) used thermal transmittance of the envelope material (U_{env}) multiplied by the difference between T_{ext} and T_{int}. Finally, the amount of stored energy, q_{stored}, is represented by Equation (11) with ρ_{env}, $c_{p_{env}}$, T_{env}, and d_{env} are the density, specific heat capacity, average temperature, and thickness of the envelope material, and t is time.

$$q_{conv\_ext} = h_{amb}(T_{amb} - T_{ext}) \tag{7}$$

$$q_{conv\_int} = h_{int}(T_{ind-air} - T_{int}) \tag{8}$$

$$h_{amb} = 2.8 + 3.0v \tag{9}$$

$$q_{cond} = U_{env}(T_{int} - T_{ext}) \tag{10}$$

$$q_{stored} = \rho_{env}\ c_{p_{env}}\ \frac{\partial T_{env}}{\partial t}\ d_{env} \tag{11}$$

3.3.2. Heat balance of the solar absorber and RC emitter

Like Equation (4) for building envelope, the heat balance for the solar absorber and RC emitter also consists of absorbed solar radiations, heat exchanges with the sky, convection, and conduction. However, there are some changes in the detailed equations for those terms, as shown in Equation (12). The absorber and emitter only receive the transmitted q_{sol} by the glass or PE cover, and thus the term becomes q_{sol_glass} and q_{sol_PE}, which are detailed in Equation (13) with the introduction of the solar transmissivity of the glass ($\tau_{glass,sol}$) and PE cover ($\tau_{PE,sol}$). The values of $\tau_{glass,sol}$ and $\tau_{PE,sol}$ used in the simulation are 92% and 90% respectively.

Similarly, the q_{rad} term in Equation (4) is modified as q_{rad_abs} and q_{rad_emit} for the absorber and emitter with the introduction of $\tau_{glass,atm}$and $\tau_{PE,atm}$ in Equation (14) as the glass and PE cover transmissivity in the infrared band (0% for the glass and 90% for the PE cover). It is worth noting that, for simplicity, the multiple reflections between the glass/PE film with the absorber/emitter are neglected because of the extremely small solar reflectivity (5%) of the absorber and PE film. Other terms in Equation (12) are similar to the previously explained Equations (7)–(11).

$$\begin{cases} q_{sol\_glass} + q_{rad\_abs} + q_{conv\_int} + q_{cond} = q_{stored}\ \text{, for absorber} \\ q_{sol\_PE} + q_{rad\_emit} + q_{conv\_int} + q_{cond} = q_{stored}\ \text{, for emitter} \end{cases} \tag{12}$$

$$\begin{cases} q_{sol\_glass} = \tau_{glass,sol}\ \alpha_{abs}\ H_{abs}\ \text{, for absorber} \\ q_{sol\_PE} = \tau_{PE,sol}\ \alpha_{emit}\ H_{emit}\ \text{, for emitter} \end{cases} \tag{13}$$

$$\begin{cases} q_{rad\_abs} = \tau_{glass,atm}\ F_{surf}\ \varepsilon_{abs}\ \varepsilon_{sky}\ \sigma\ (T_{sky}^4 - \ T_{abs}^4)\ \text{, for absorber} \\ q_{rad\_emit} = \tau_{PE,atm}\ F_{surf}\ \varepsilon_{abs}\ \varepsilon_{sky}\ \sigma\ (T_{sky}^4 - \ T_{emit}^4)\ \ \text{, for emitter} \end{cases} \tag{14}$$

3.4. Grid and time-step independence study

Results of the simulation parameters from five combinations of grid and time-step sizes were compared. As shown in Fig. 6, it is clear that the indoor air temperature and velocity results among the grid and time step sizes do not vary too much, with average relative variations between the mesh and time step sizes of 0.2 °C for temperature and 0.02 m/s for velocity. However, the hourly flow rate results differ largely for coarser grid sizes, and it only becomes stable from the 1 cm grid size and 450 s time step size, with relative variations of 0.01 m^3/s. Therefore, this grid and time step size (1 cm and 450 s) were used for the parametric study simulation.

3.5. Simulation validation

Two features of our simulation need to be validated: the heat transfer model and the airflow model. For the heat transfer model validation, we used experimental data from a double-covered photothermal and radiative cooling (PT-RC) module by Hu et al. [63]. The PT-RC module was a solar collector during the daytime and an RC emitter at night-time, which is considered appropriate to check our heat transfer models that also include both solar absorption and thermal radiation. The comparison between the simulation results and the experimental data is shown in Fig. 7 for the (a) glass temperature and (b) absorber temperature. Quantitative assessment of the simulation results using the root mean square deviation (RMSD) [63,64] as in Equation (1), with $X_{sim,i}$ as the simulation data point and $X_{exp,i}$ as the experimental data point, shows a good conformity between the simulation and experiment. The RMSD of the simulated glass temperature and absorber temperature are 0.8% and 1.7%, respectively.

$$RMSD = \sqrt{\frac{1}{n}\sum_{i=1}^{n}\left[\frac{(X_{sim,i} - X_{exp,i})}{X_{exp,i}}\right]^2} \tag{1}$$

Moreover, to validate our ventilation flow model, we compared the simulation results with experimental data from an SC study by Chen et al. [34]. The SC in Chen et al. experiment was a 1.5 m high SC that was uniformly heated at one of the surfaces. In one of their tests, they measured the air temperature, velocity, and flow rate for a 20 cm channel gap and 45° inclination angle, which is similar to our case study building. Thus, we compared the data from this specific experimental setup. Results for the temperature and velocity profiles are summarised in Fig. 8. Overall, all the parameter profiles resulting from the simulation show close values with the experimental data with RMSD values for temperature and velocity distributions inside the chimney of 3% and 14%, respectively. Dissimilarities between the simulation and experiment are observed in velocity distribution near the walls (Fig. 8 (b)), possibly due to the discrepancy from the near-wall treatment model. Nonetheless, the airflow rate resulting from the simulations still shows a good agreement with the experiment, including the flow rate (0.037 m^3/s compared to 0.035 m^3/s from the experiment).

4. Results and discussion

Analysis of the effect of different parameters on the performance of SC-RC is conducted by comparing two primary variables, i.e., the cooling performance and ventilation performance. The cooling performance is indicated by the difference between indoor air temperature with ambient temperature ($\Delta T_{room} = T_{room} - T_{amb}$). Whereas the ventilation performance is analysed using the flow rate through the RC cavity (m^3/s) and the total ventilation rate in both m^3/s and ACH.

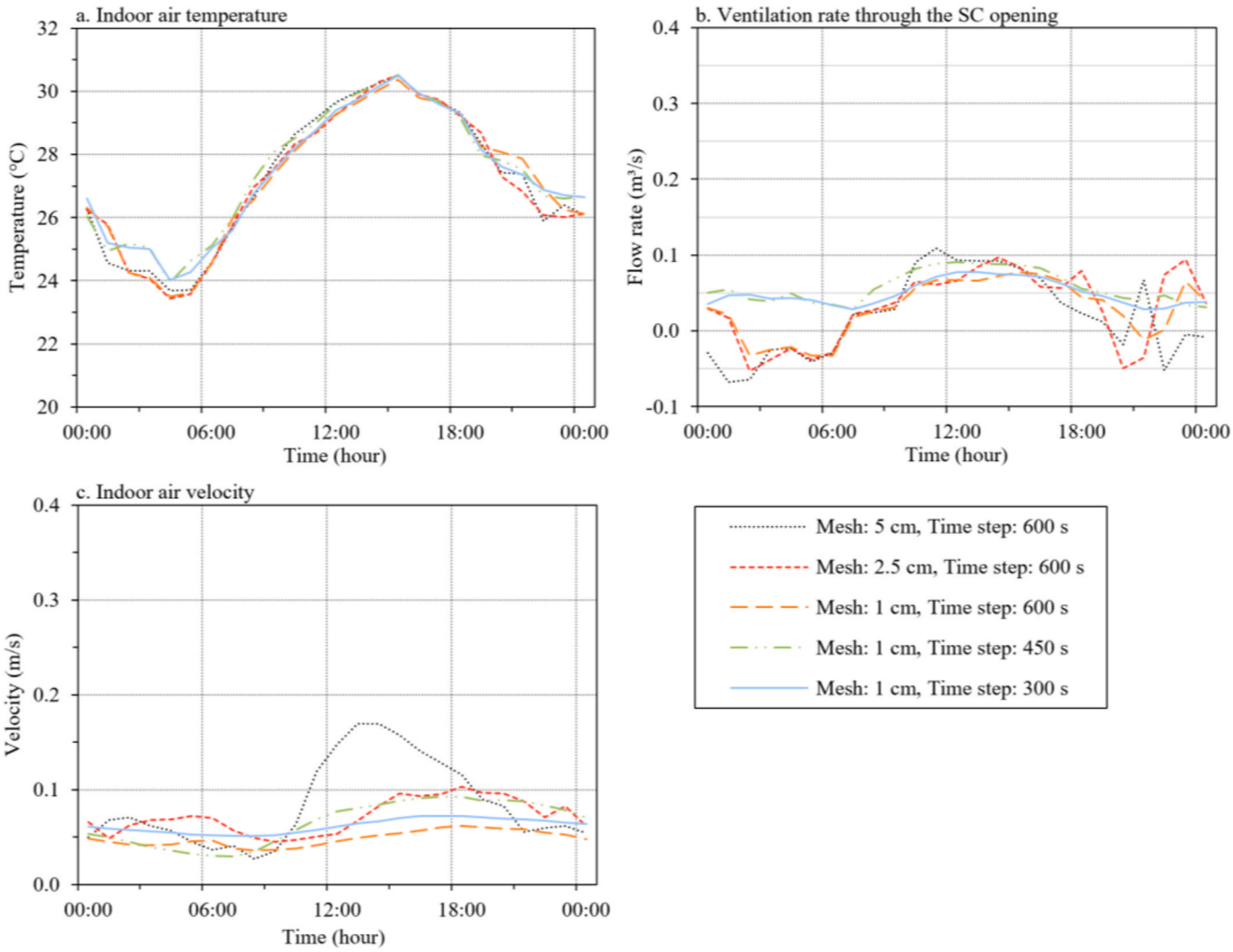

Fig. 6. Comparison of hourly pattern of (a) indoor air temperature, (b) volume flow rate through the SC opening, and (c) indoor air velocity resulting from the different grid and time step sizes.

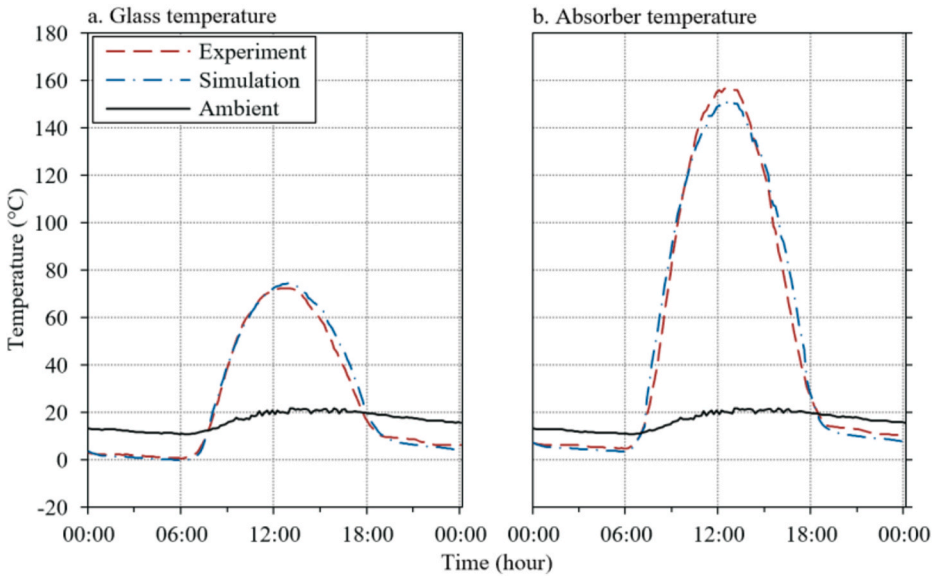

Fig. 7. Comparison of experimental and simulation results of the PT-RC: (a) glass temperature and (b) absorber temperature.

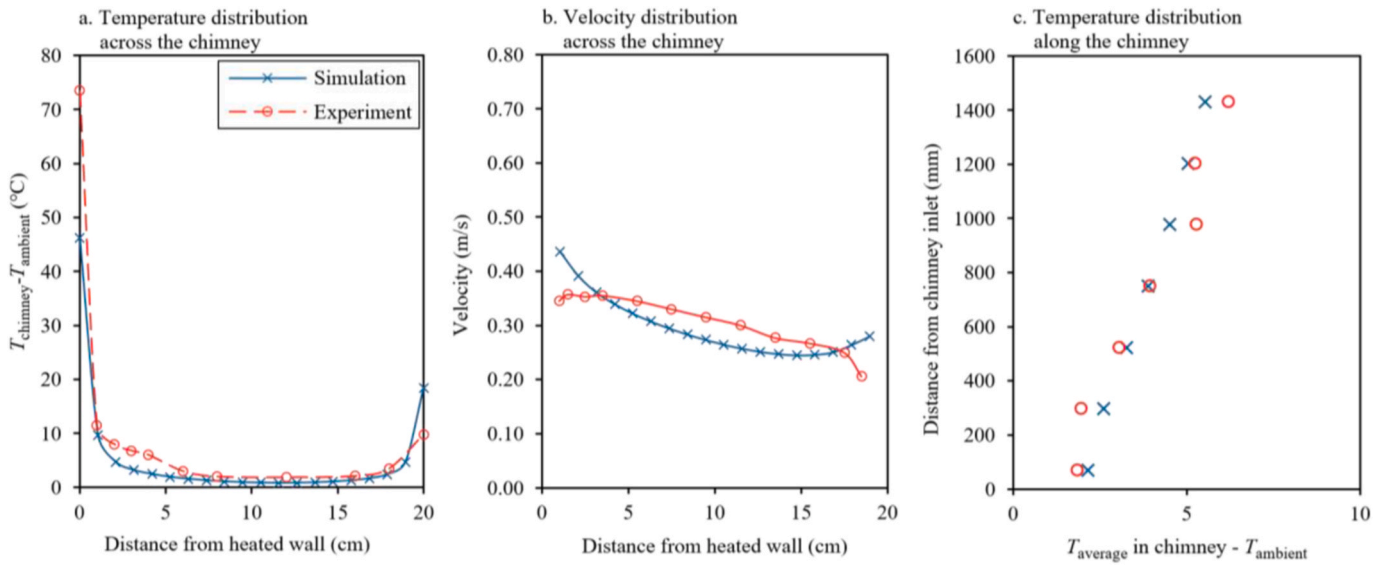

Fig. 8. Comparison between the SC simulation and the experimental data [34]: (a) temperature and (b) velocity distribution across the solar chimney, and (c) temperature distribution along with the solar chimney.

4.1. *Effect of RC emitter's convection cover*

Incorporating PE cover has a noticeable effect mainly on the RC emitter temperature. Fig. 9 (a) shows that the PE-covered RC emitter's temperature is around 2 °C lower than the uncovered RC emitter. In fact, the temperature of the PE-covered RC emitter is consistently sub-ambient throughout the day, whereas the uncovered RC loses its cooling power in the high solar radiation period between 10 a.m. and 5 p.m. The emitter temperature data also imply that the PE-covered SC-RC can provide a lower room temperature than the uncovered SC-RC, and Fig. 9 (b) confirms this with ΔT_{room} gap of −0.39 °C between the two cases. A distinctive pattern of hourly ΔT_{room} between PE-covered SC-RC with the uncovered SC-RC and the reference case SC can also be recognised from Fig. 9 (b). The PE-covered SC-RC creates a sub-ambient room for a longer period (3 h longer) than the uncovered SC-RC or the reference case SC.

For ventilation performance analysis, Fig. 10 reveals that in the daytime, there is a reversed flow in the RC cavity of the uncovered SC-RC, indicated by negative flow rate values between 11 a.m. and 6 p.m. During this period, the cooling effect from the uncovered RC emitter is not enough to generate a downward flow of natural convection; rather, the warmer room air due to solar heat gain can force an upward flow in the RC cavity. Therefore, the uncovered SC-RC has a warmer room on average than the PE-covered SC-RC. Despite those variations in RC cavity flow, both the PE-covered and uncovered SC-RC have a comparable ACH value of 2.0 and 2.1, respectively, higher than the SC-only case with 1.8 ACH. However, the total flow rate data in Fig. 10 shows that the uncovered SC-RC is more identical to the SC pattern than the PE-covered SC-RC, especially in the daytime when an upward RC cavity flow occurs in the uncovered SC-RC. Thus, the PE-covered SC-RC is preferable because it can provide more ACH and cool air to the room.

4.2. *Effect of building's thermal mass*

In real situations, most buildings use heavyweight and long-lasting materials for their wall, such as brick, stone, or concrete. These materials are considered thermal mass materials that can absorb heat slowly and store it for some time before releasing it later and supposedly affect the performance of the SC-RC ventilation. Figs. 11 and 12 compare the cooling and ventilation performance of PE-covered SC-RC with a brick wall (the base case) and a lightweight insulation board wall, as well as the reference case (SC with a brick wall). As Fig. 11 shows, thermal mass shifts the starting point of warmer ΔT_{room} from 1 p.m. in the lightweight wall case to 7 p.m. in the base case. This might be beneficial since the ambient temperature in the afternoon is higher than in the evening, so it is better not to have a warmer room in the afternoon. Despite the shifting in the warm ΔT_{room} period, there is no apparent difference in the daily average ΔT_{room} of the base SC-RC and SC-RC with light wall, with the base case has a slightly better cooling performance (−0.30 °C compared to −0.29 °C).

In terms of flow rate through the RC cavity, the base case SC-RC can match the total ACH provided by the SC-RC with light wall materials, with a <0.1 ACH difference (see Fig. 12). Despite this similar ACH, the flow pattern from the two cases is distinctive. In the lightweight-walled SC-RC case, the RC cavity flow rate peaks before noon and plunges early evening. These maximum and minimum flow rates in the RC cavity are shifted and reduced in the SC-RC with thermal mass, with the maximum shifted to 3 h later (at 2 p.m.) and the minimum to 6 h later (at 3 a.m.). The thermal mass wall's heat storage capacity makes it release the daytime heat gain to the night. The released heat creates a warmer room with a conflicting flow tendency (upward flow) with the cool RC cavity (downward flow). Therefore, the RC flow rate is lower for the base case than the light wall case, and consequently, the base case SC-RC with a heavy wall has a slightly lower daily ACH. Nevertheless, the long-lasting heavyweight wall with a minuscule difference in ACH and a better cooling effect is more prevalent in practice than the lightweight wall.

4.3. *Effect of RC cavity gap*

A narrower RC cavity gap is expected to exchange heat between the RC emitter and the cavity air better, resulting in a cooler air temperature from the RC cavity. This is evident in the ΔT_{room} data from different RC cavity gaps are shown in Fig. 13. Cavity with a 10 cm gap produces the lowest room temperature, with −0.41 °C lower than ambient on a daily average. The cooling effect from the RC cavity to the room diminishes as the RC cavity gap gets wider, although, with a cavity gap of 30 cm, the SC-RC ventilation still cools the room slightly better than the SC-only case with a daily average ΔT_{room} of −0.23 °C lower than the SC only.

Unlike the appealing effect for cooling performance from the narrower cavity gap, the ventilation performance shows the opposite result. Fig. 14 shows the flow rate through the RC cavity and the total ventilation flow (in m^3/s and ACH). The flow rate through the RC cavity gradually increases with the wider cavity gap, which is observed both in the hourly and daily average rates. The total ventilation rate also shows

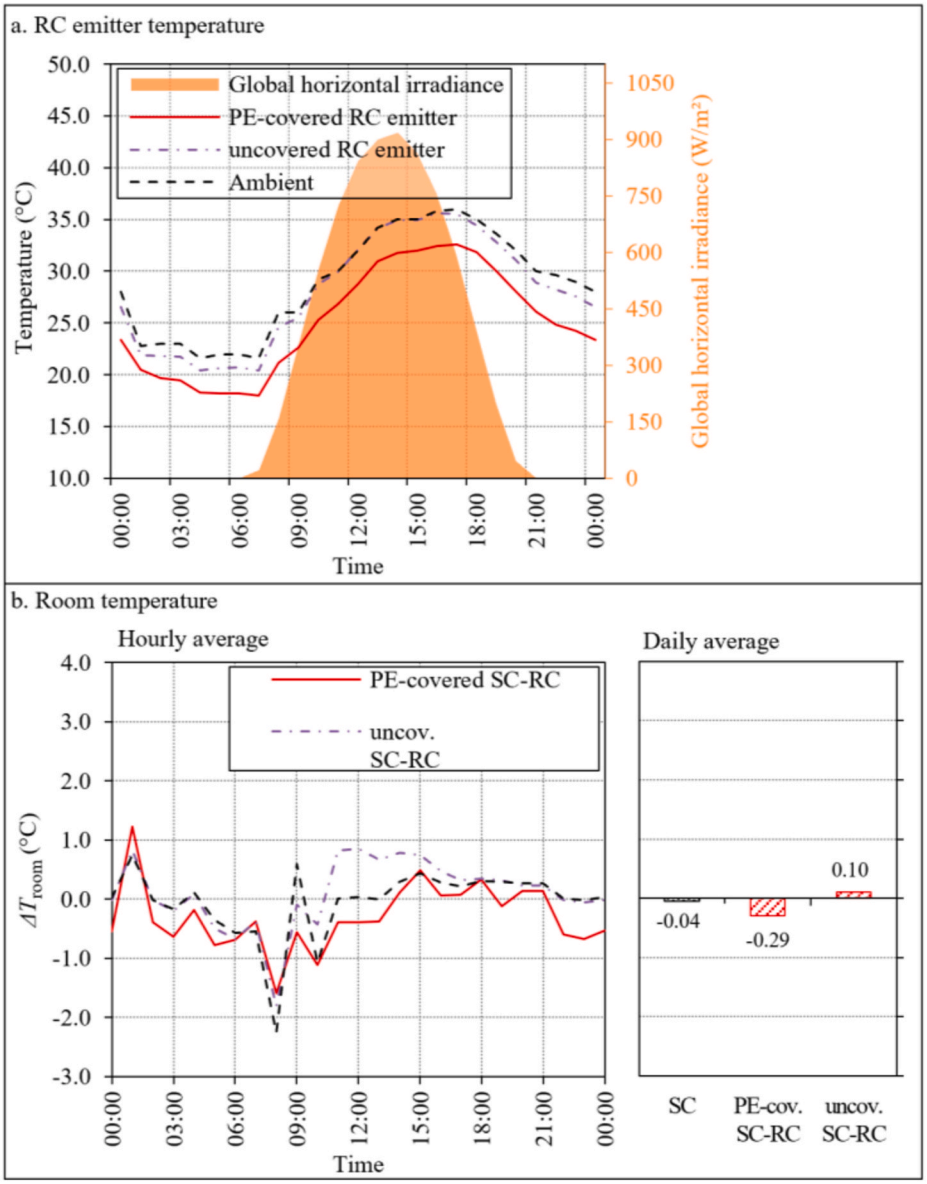

Fig. 9. (a) RC emitter's temperature and (b) Hourly and daily average ΔT_{room} of SC-RC with and without PE cover.

a similar trend with the RC cavity flow, with an average 0.14 ACH improvement per 5 cm gap enlargement. The widest gap of 30 cm RC cavity provides up to 2.19 ACH, but the narrowest cavity gap (10 cm) of the SC-RC ventilation only has a negligible improvement of 0.01 ACH compared to SC ventilation.

4.4. *Effect of internal heat gain*

Heat gains, external and internal, are the cause of the temperature increase in a room, therefore increasing internal heat gain raises ΔT_{room} to be warmer. Nevertheless, a comparison of the effect of different internal heat gains to ΔT_{room} is still relevant to know at what level of internal heat gain the SC-RC still gives a sub-ambient daily average ΔT_{room}. Fig. 15 shows the expected increase in ΔT_{room} as the internal heat gain increases, and it also reveals that with some internal and solar heat gain, conventional SC ventilation cannot help to cool the indoor environment. Meanwhile, the SC-RC has some cooling capacity to create a sub-ambient room temperature with internal heat gain reaching 4 W/m^2. The discrepancies of ΔT_{room} between SC and SC-RC ventilation is bigger in the higher internal heat gain condition, with −0.24 °C ΔT_{room} gap in 0 W/m^2 to −0.29 °C in 4 W/m^2.

Furthermore, Fig. 16 indicates that a warmer room limits the RC cavity flow due to increased internal heat gain. The flow rate delivered from the RC cavity shown in Fig. 16 has a decreasing trend with a reduction of 0.008 m^3/s daily average RC flow rate as the internal heat gain raised by 4 W/m^2. However, in the case of increasing internal heat gain, the total ACH seems stable (around 1.9 ACH) as the heat gain increases. This stable ACH means that only the contribution of the RC cavity for ventilation is reduced, while the contribution of SC is raised with the rise of internal heat gain. It can be observed in the widening gap between the ACH line and the RC cavity flow line in the early evening in Fig. 16. Therefore, it will follow that, at a particular value of internal heat gain (>4 W/m^2), the RC cavity will no longer be able to produce a downward flow. Instead, it becomes a channel for an upward flow.

4.5. *Effect of climate and geographical location*

Among the five climate types that need cooling, three climates resemble dry conditions with a high clear sky index. In these types of climates, namely BSh, BWh, and Csa, RC works best, which is confirmed

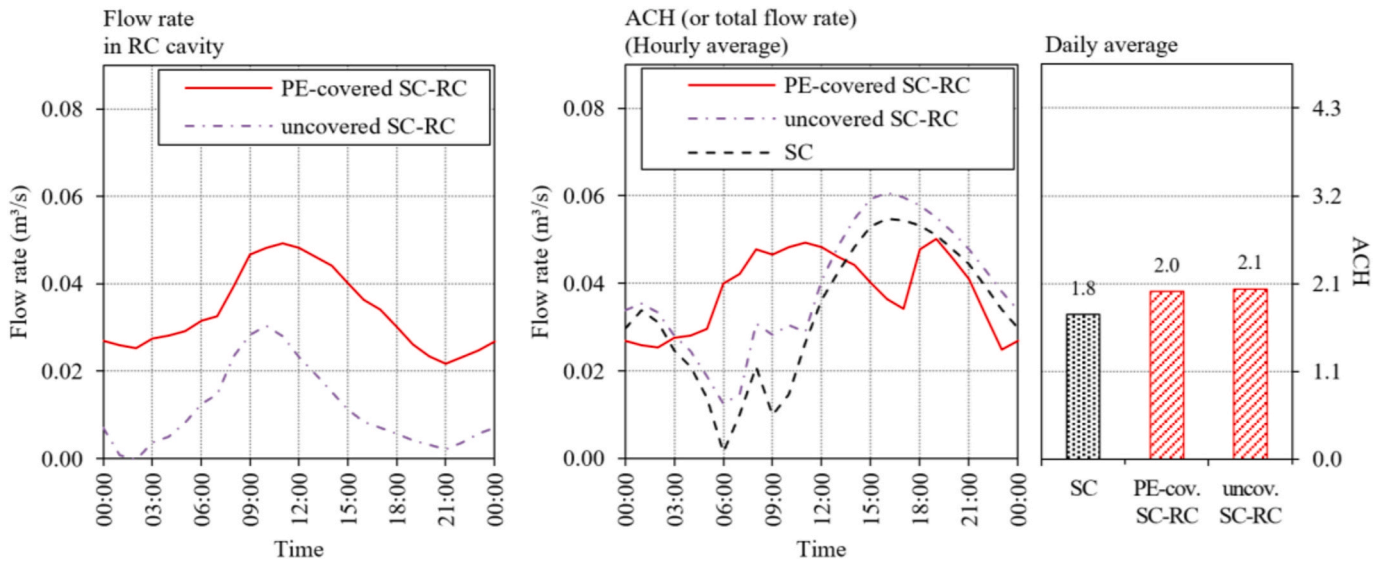

Fig. 10. RC cavity and total flow rate of SC-RC with and without PE cover.

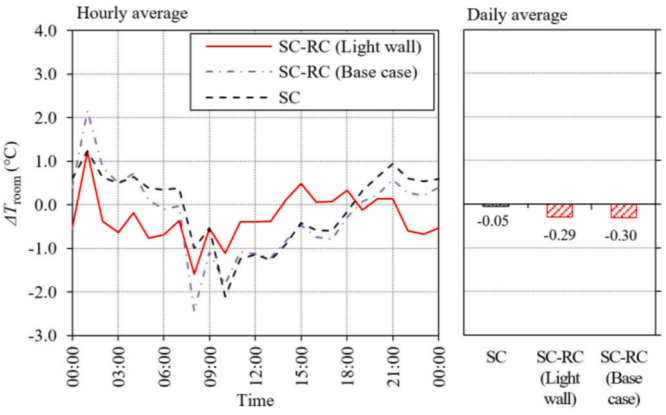

Fig. 11. ΔT_{room} of SC-RC with different wall materials.

by Figs. 17 and 18. In Fig. 17, all climates seem to have a sub-ambient daily average ΔT_{room}, but with a different hourly pattern. However, in both humid climates, tropical humid (Af) and temperate humid (Cfa), ΔT_{room} is limited to be around −0.5 °C at best, and the daily average ΔT_{room} are −0.07 °C and −0.06 °C respectively. In the drier climates, on the other hand, ΔT_{room} can reach −2 °C or more, with the lowest possible ΔT_{room} found in Csa climate. Although Csa has the lowest ΔT_{room}, BSh and BWh climate are more stable to give hourly sub-ambient room temperature (18 h of sub-ambient ΔT_{room}) and hence they have the lowest daily average ΔT_{room} with −0.46 °C and −0.56 °C, respectively.

Consistent with the cooling performance, the ventilation performance of SC-RC ventilation is better in the three dry climates (see Fig. 18). In the tropical and temperate humid, the flow rate through the RC is even lower than the flow rate through an SC in the SC-only case most of the time, resulting in their daily average ACH being lower than in the SC-only case. This inferior performance from the SC-RC in the humid regions can be explained using the data in Fig. 17. The ΔT_{room} for the SC ventilation in both Af and Cfa are positive, while their respective ΔT_{room} for the SC-RC are effectively zero, a supportive condition for an

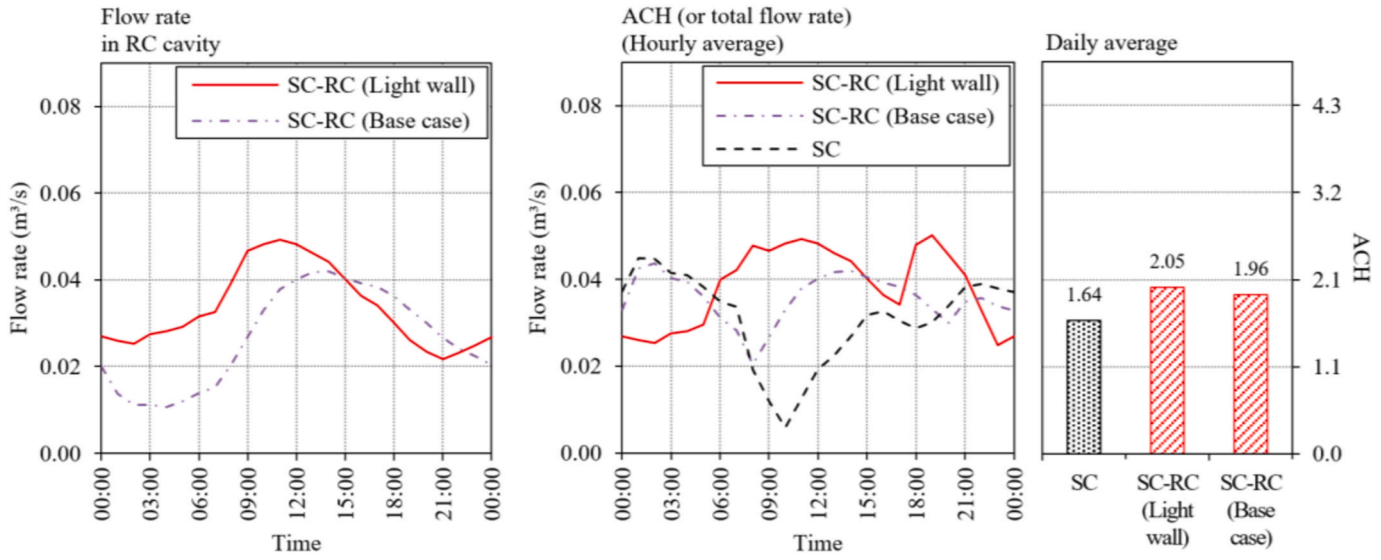

Fig. 12. RC cavity and total flow rate of SC-RC with different wall materials.

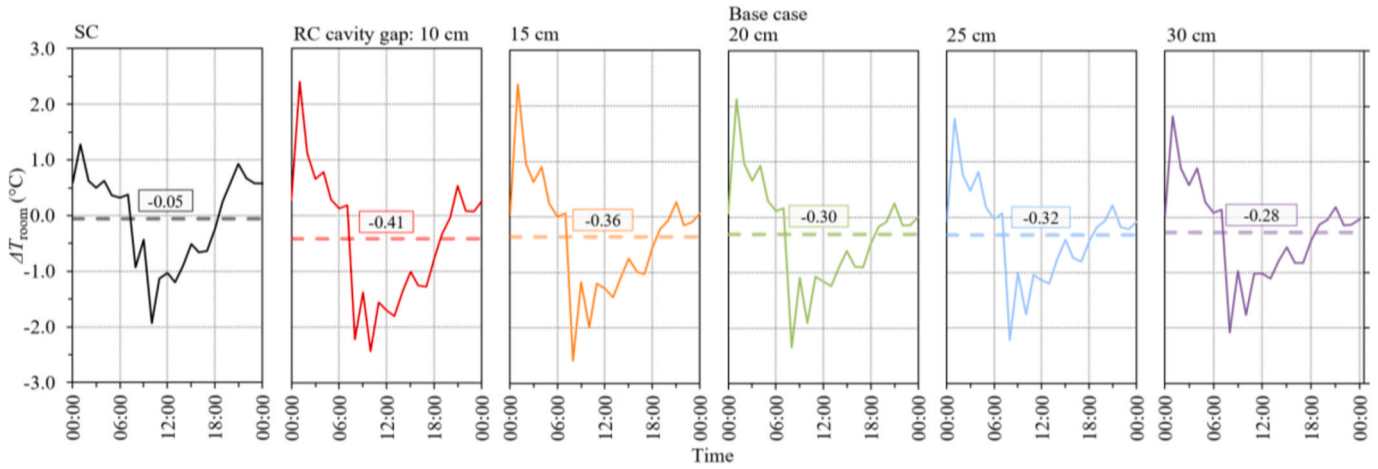

Fig. 13. ΔT_{room} of SC-RC with different RC cavity gaps.

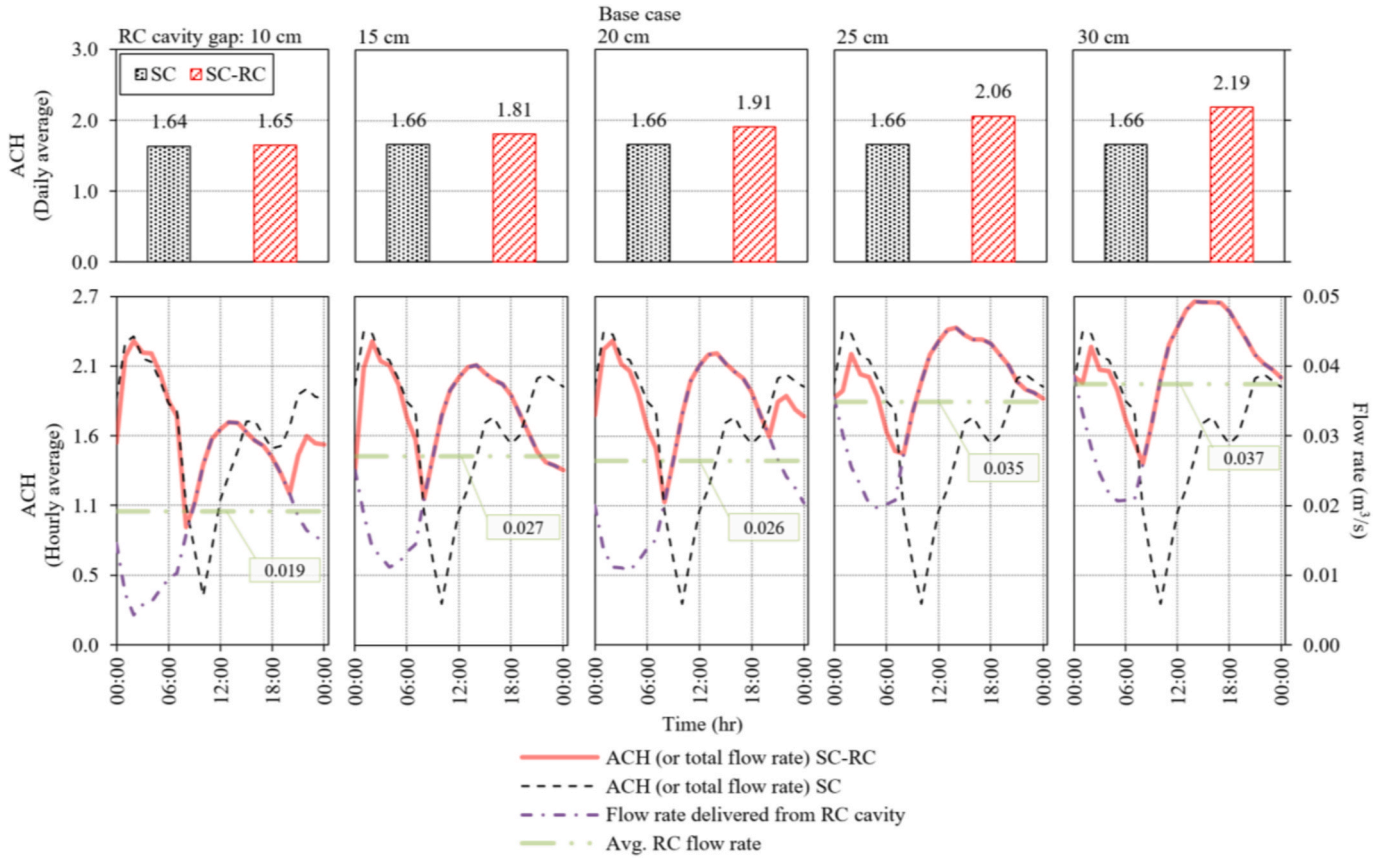

Fig. 14. RC cavity and total flow rate of SC-RC with different RC cavity gaps.

upward flow through the SC rather than a downward flow through the RC cavity. This shows that the SC-RC ventilation may not be suitable for enhancing the SC ventilation in humid climates. Whereas in the other drier climates, the total flow rate of the SC-RC ventilation can exceed the SC ventilation. Also, the total ACH of the BSh, BWh, and Csa climates are better than the SC-only case, with ACH improvement of 0.6, 0.4, and 0.4, respectively.

4.6. *Effect of using a fan to help the flow rate in the RC cavity*

When a fan is considered to help the flow in the RC cavity, it is expected that there is an optimal daily average fan flow rate to get the maximal cooling effect from the RC emitter surface. Nevertheless, the ΔT_{room} data shown in Fig. 19 reveals that the optimal RC flow rate to get the lowest ΔT_{room} is different for different climates. Fig. 19 demonstrates that adding a fan does not increase their cooling performance in climates where the SC-RC performs better than the SC ventilation. It means that using the SC-RC in a naturally ventilated (NV) system is a better option than a fan-assisted one in these dryer climates (BSh, BWh, and Csa). However, for humid climates where the SC-RC ventilation performs worse, a fan-assisted SC-RC may improve the cooling power of the RC cavity with 0.1 °C ΔT_{room} reduction at the optimal daily average fan flow rate of 0.05 m^3/s. When the daily average fan flow rate increases to 0.1 m^3/s in these two humid regions, the cooling performance is still slightly

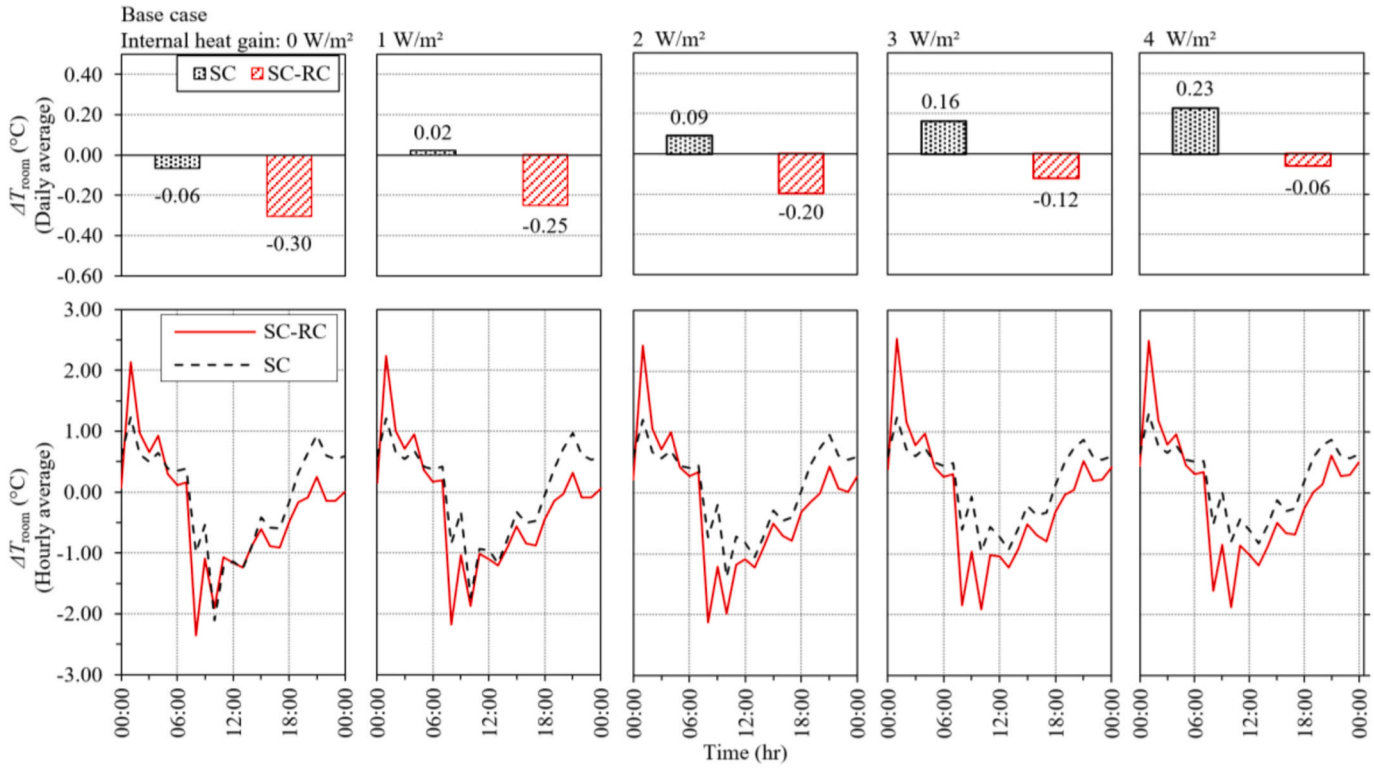

Fig. 15. ΔT_{room} of SC-RC with different room's internal heat gains.

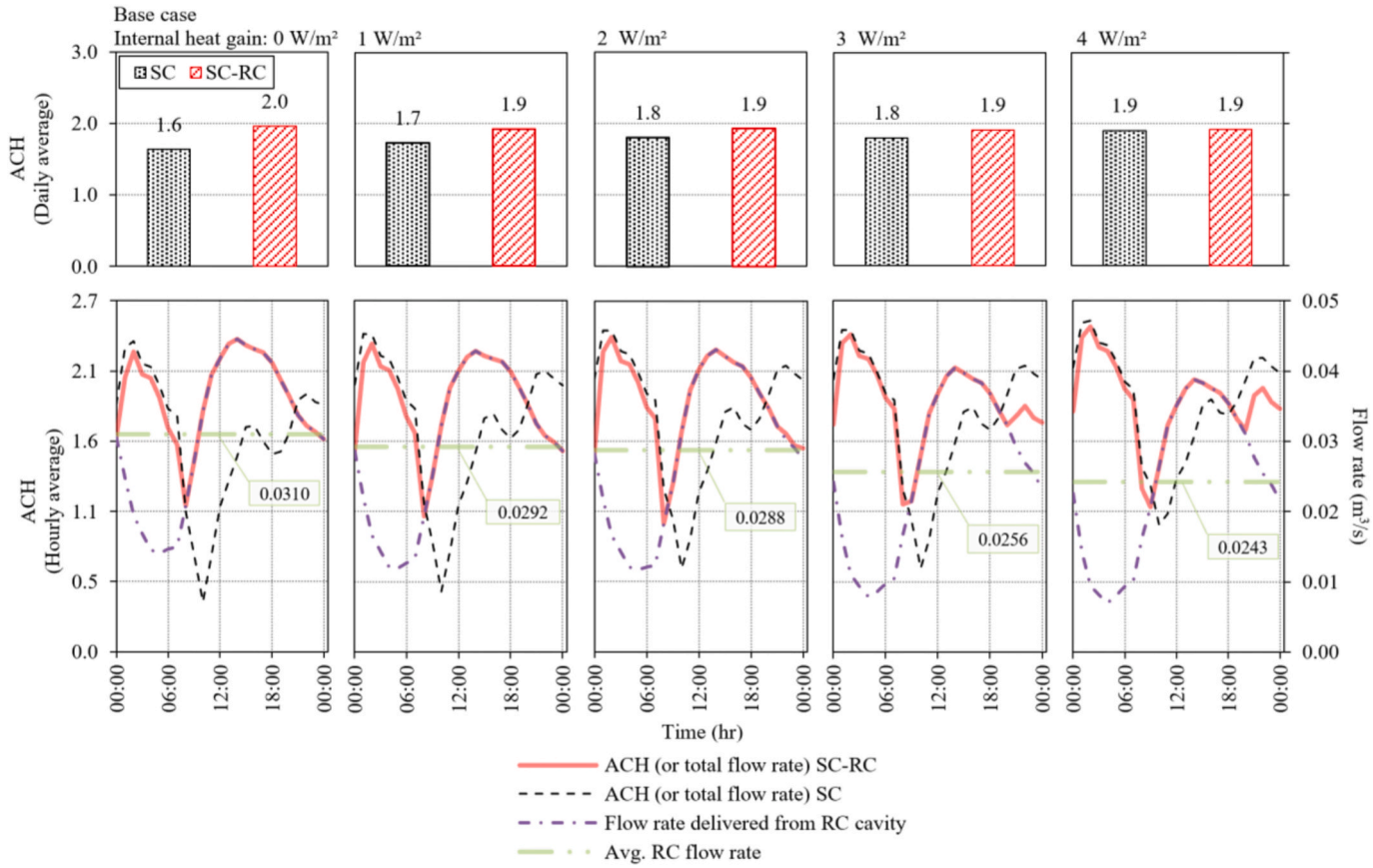

Fig. 16. RC cavity and total flow rate of SC-RC with different room's internal heat gains.

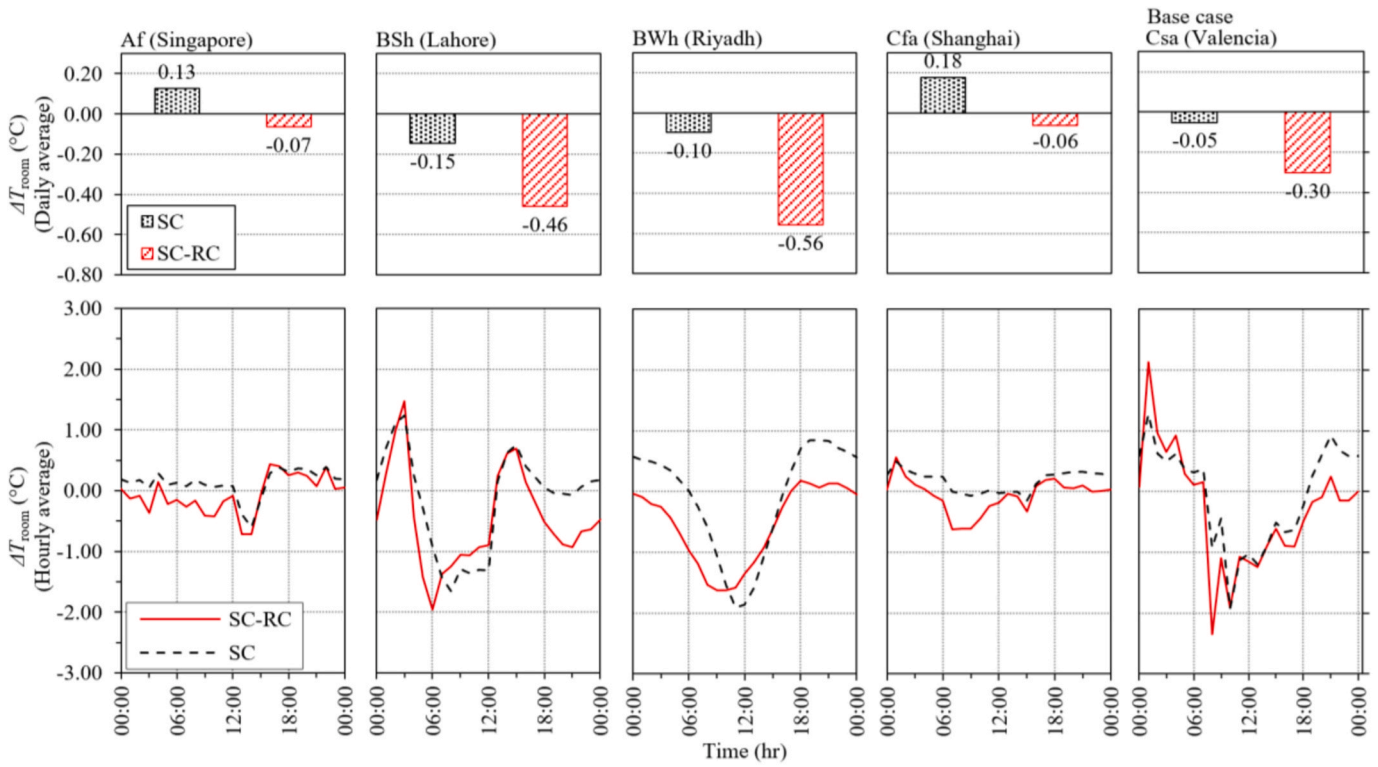

Fig. 17. ΔT_{room} of SC-RC in different climates.

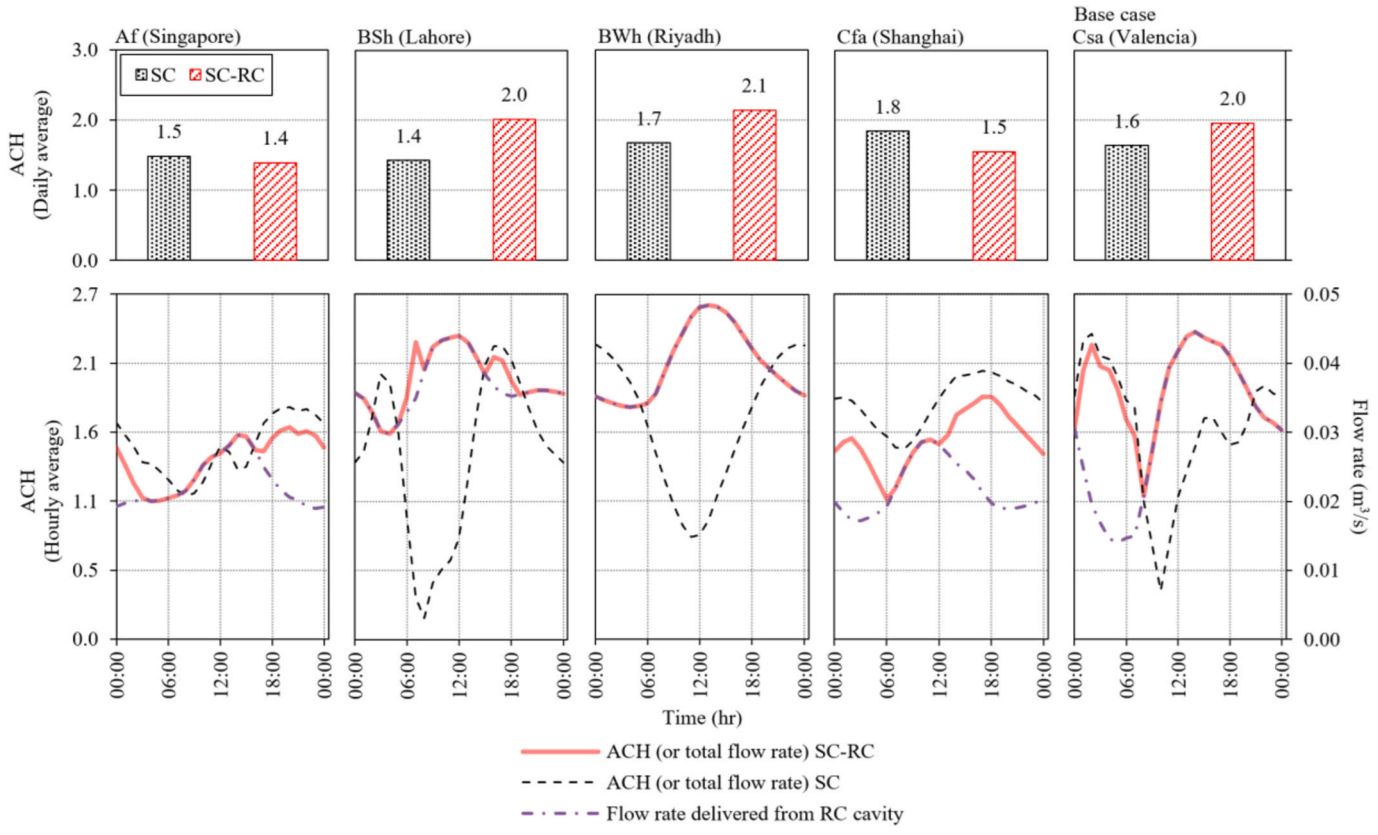

Fig. 18. RC cavity and total flow rate of SC-RC in different climates.

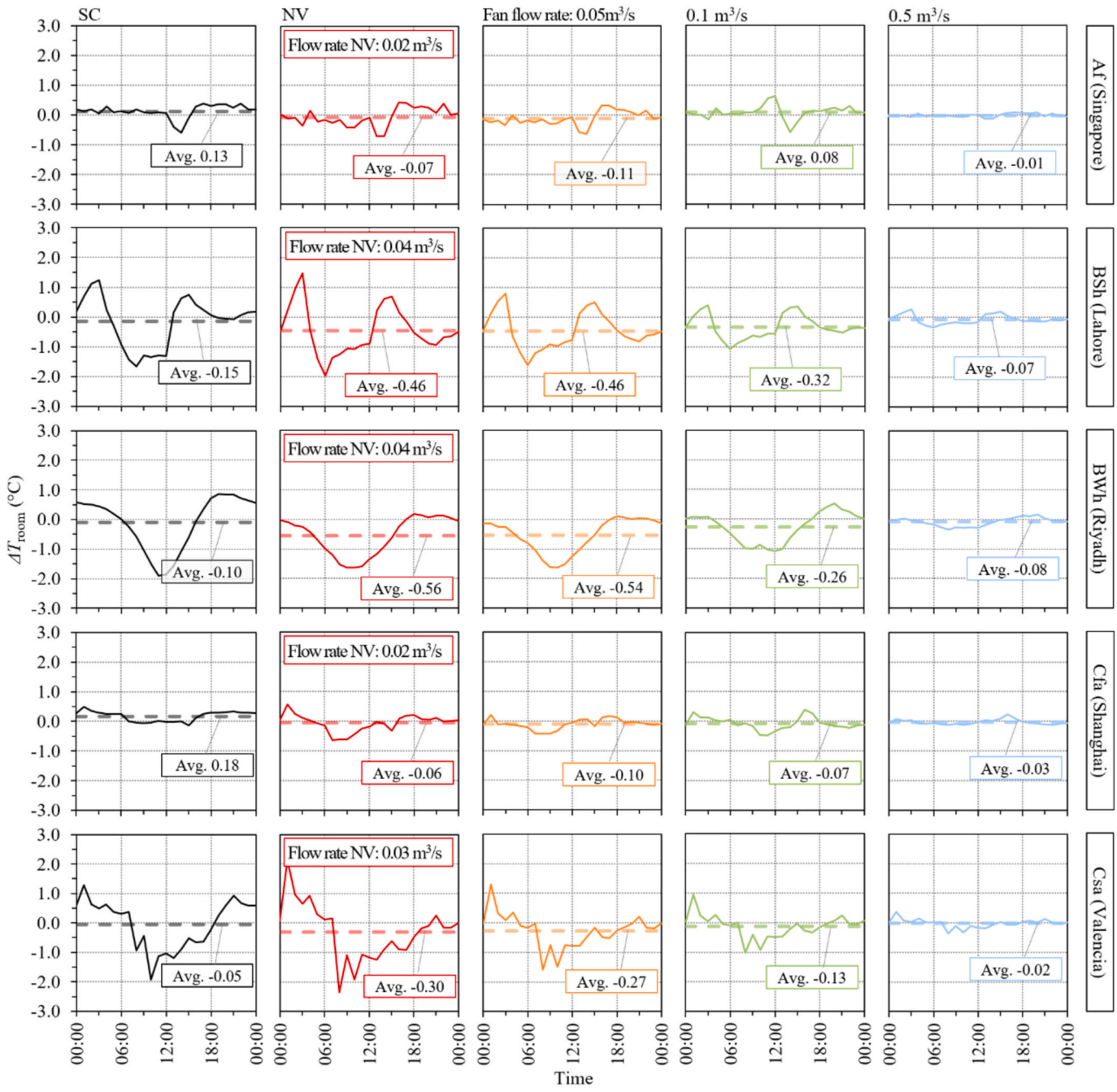

Fig. 19. ΔT_{room} of SC-RC in different locations with different fan power.

better than in the NV case, but a daily average fan flow rate higher than 0.1 m^3/s will not be effective in providing sub-ambient ΔT_{room}.

5. Conclusion

In a conventional gabled roof SC ventilation, the SC is placed on the sun-faced side of the roof while the opposite side is idle. On this sun-opposite side of the roof, an RC cavity can be set to assist and improve the performance of the SC ventilation. It is found that the RC cavity in this SC-RC ventilation system can increase the ventilation rate by up to 2.1 ACH and reduce the room temperature by up to 2°. Furthermore, the effect of six influential parameters on the performance of the SC-RC ventilation is studied, and the findings are summarised below.

- The PE cover that protects an RC emitter from convection heat loss, as well as a thermal mass that helps regulate the building's external heat gain, positively impacts the ventilation and cooling performance of the SC-RC ventilation.
- The narrow RC cavity gap cools the inlet air but reduces the flow rate. Practically, one could use an RC air gap similar to the SC (20 cm) for optimal cooling and ventilation performance.
- Building's internal heat gain limits the cooling performance from the RC cavity to produce a sub-ambient room temperature. At 4 W/m^2 internal heat gain, considered a high internal heat gain for a typical building, the capability of SC-RC to produce sub-ambient room temperature slowly diminishes. This warmer room, along with the rise in internal heat gain, also causes the RC cavity flow rate to reduce. It is predicted that at a remarkably high internal heat gain level, the RC cavity will no longer be able to produce a downward

flow and starts acting as a channel for an upward flow. Nevertheless, in all those parameters mentioned above, the cooling and ventilation performances of SC-RC are better than the SC-only case.

- In addition, the performance enhancement of the SC-RC compared to the SC is not achieved in all climates. Among the five warmest climatic types, the SC-RC performs better than the SC in three dry regions such as steppe (BSh: Lahore), desert (BWh: Riyadh), and dry temperate climate (Csa: Valencia). SC-RC produces the best cooling and ventilation performance in the two driest climates, BSh (Lahore) and BWh (Riyadh), with a daily average ΔT_{room} of -0.46 °C and -0.56 °C, respectively, and more than 0.4 ACH improvement from the SC ventilation, to be 2.0 ACH and 2.1 ACH, respectively. Also, in those climates where RC performs best, adding a fan may only increase the flow rate but also diminishes the cooling capability of the RC cavity.

Nonetheless, this study also has some limitations. Firstly, excluding the wind effect on the ventilation may contribute a significant difference when wind-forced ventilation is involved. Secondly, the model assumed that the west and east walls are well-insulated, so the effect of external heat gains from these walls on the flow pattern is neglected. This assumption may not be appropriate for relatively small room sizes. Thirdly, specifically located internal heat gain sources may create a different flow pattern than the uniformly distributed internal heat gain set in the simulation.

Moreover, for future studies, the influence of other design features related to buildings may be investigated, such as the roof shape, opening locations, building plan and geometry, number of floors, etc., on the performance of this natural ventilation strategy. Further study on the effectiveness of the SC-RC ventilation in various building types and functions according to an occupation schedule can also reveal additional advantages and disadvantages of this ventilation strategy.

CRediT authorship contribution statement

Suhendri Suhendri: Writing – review & editing, Writing – original draft, Methodology, Formal analysis, Conceptualization. **Mingke Hu:** Writing – review & editing, Supervision, Conceptualization. **Yuehong Su:** Writing – review & editing, Supervision, Conceptualization. **Jo Darkwa:** Supervision. **Saffa Riffat:** Supervision.

Declaration of competing interest

The authors declare that they have no known competing financial interests or personal relationships that could have appeared to influence the work reported in this paper.

Data availability

Data will be made available on request.

Acknowledgments

This research was supported with a Ph.D. studentship (Reference number: S-2401/LPDP.4/2019) funded by Indonesia Endowment Fund for Education (Lembaga Pengelola Dana Pendidikan), Ministry of Finance, Republic of Indonesia, the National Natural Science Foundation of China (Grant number: 51906241), and the H2020 Marie Skłodowska-Curie Actions-Individual Fellowships (Grant number: 842096).

Appendix. Ansys Fluent Settings

- ➢ General: pressure-based solver, transient simulation
- ➢ Energy: On
- ➢ Viscous model: Standard $k-\varepsilon$ turbulence model with standard wall function
- ➢ Radiation model: Discrete ordinates with 4 radiation bands (Band 0: 0.2–3 μm; Band 1:3–8 μm; Band 2: 8–13 μm; Band 3: 13–25 μm)
- ➢ Materials

Material	Thermal properties		
	Thermal conductivity ($W \cdot m^{-1} \cdot K^{-1}$)	Density ($kg \cdot m^{-3}$)	Specific heat capacity ($J \cdot kg^{-1} \cdot K^{-1}$)
Air	Piecewise linear 250 K: 0.0223 300 K: 0.0263 350 K: 0.03 400 K: 0.0338	Incompressible ideal gas law	Piecewise linear 250 K: 1006 300 K: 1007 350 K: 1009 400 K: 1014
Ground	0.364	1600	800
Brick	0.72	1920	840
Ceramic tile	0.8	1700	850
Insulation board	0.033	38	1400
Roof tile	0.8	1890	880
Timber	0.16	720	1260
Absorber	202.4	2719	871
Glass	1.38	2203	703
Emitter	202.4	2719	871

- ➢ Cell Zone Conditions:
  - o Operating pressure: 101325 Pa
  - o Gravity in Y direction -9.81 m/s^2
  - o Operating temperature: Ambient temperature
  - o Outdoor air condition: Ambient temperature
  - o Indoor air condition: Solar fenestration and internal heat gain
- ➢ Boundary condition

Boundary name	Type (Material)	Thermal Boundary conditions	Radiation Boundary Conditions
External domain			
Top boundary	Pressure outlet	Total temperature: T_{amb}	0
Side boundary	Pressure outlet	Total temperature: T_{amb}	0
Ground	Wall (Ground)	Mixed Heat transfer coefficient: h_{amb} Free stream temperature: T_{amb} External emissivity: ε_{sky} External radiation temperature: T_{sky}	Internal emissivity Band 0: 0.7 Band 1: 0.87 Band 2: 0.97 Band 3: 0.98
Building domain			
SC opening, RC opening, and Wall opening	Internal	-	-
Roof	Two-sided Wall (Roof tile)	Coupled; External heat sources in Equation (2), namely $q_{sol} + q_{rad} + h_{amb}(T_{amb} - T_{surf})$, are inputted in the Heat Generation Rate entry-box*	Internal emissivity Band 0: 0.87 Band 1: 0.93 Band 2: 0.95 Band 3: 0.95
Glass	Two-sided Wall (Glass)	Coupled; External heat sources in Equation (2), namely $q_{sol} + q_{rad} + h_{amb}(T_{amb} - T_{surf})$, are inputted in the Heat Generation Rate entry-box*	Internal emissivity Band 0: 0.05 Band 1: 0.88 Band 2: 0.88 Band 3: 0.88
PE cover	Two-sided Wall (PE film)	Coupled; External heat sources in Equation (2), namely $q_{sol} + q_{rad} + h_{amb}(T_{amb} - T_{surf})$, are inputted in the Heat Generation Rate entry-box*	Internal emissivity Band 0: 0.05 Band 1: 0.05 Band 2: 0.05 Band 3: 0.05
RC emitter	Two-sided Wall (Aluminium)	Coupled; External heat sources in Equation (2), namely $q_{sol} + q_{rad\_emit}$, are inputted in the Heat Generation Rate entry-box*	Internal emissivity Band 0: 0.05 Band 1: 0.05 Band 2: 0.95 Band 3: 0.05
RC cavity wall	Two-sided Wall (Aluminium)	Coupled	Internal emissivity Band 0: 0.05 Band 1: 0.05 Band 2: 0.95 Band 3: 0.05
Absorber	Two-sided Wall (Aluminium)	Coupled; External heat sources in Equation (7), namely $q_{sol\_glass} + q_{rad\_abs}$, are inputted in the Heat Generation Rate entry-box*	Internal emissivity Band 0: 0.95 Band 1: 0.95 Band 2: 0.95 Band 3: 0.95
South wall	Two-sided Wall (Brick)	Coupled; External heat sources in Equation (2), namely $q_{sol} + q_{rad} + h_{amb}(T_{amb} - T_{surf})$, are inputted in the Heat Generation Rate entry-box*	Internal emissivity Band 0: 0.79 Band 1: 0.77 Band 2: 0.93 Band 3: 0.93
Window	Two-sided Wall (Glass)	Coupled; External heat sources in Equation (2), namely $q_{sol} + q_{rad} + h_{amb}(T_{amb} - T_{surf})$, are inputted in the Heat Generation Rate entry-box*	Internal emissivity Band 0: 0.05 Band 1: 0.88 Band 2: 0.88 Band 3: 0.88
North wall	Two-sided Wall (Brick)	Coupled; External heat sources in Equation (2), namely $q_{sol} + q_{rad} + h_{amb}(T_{amb} - T_{surf})$, are inputted in the Heat Generation Rate entry-box*	Internal emissivity Band 0: 0.79 Band 1: 0.77 Band 2: 0.93 Band 3: 0.93
Floor	Wall (Ceramic tile)	Heat Flux: 0	Internal emissivity Band 0: 0.34 Band 1: 0.94 Band 2: 0.93 Band 3: 0.93
Ceiling	Wall (Timber)	Heat Flux: 0	Internal emissivity Band 0: 0.46 Band 1: 0.9 Band 2: 0.94 Band 3: 0.96

**Because the Heat Generation Rate entry-box uses a volumetric unit, W/m^3, thus we need to convert the external heat source equation of the surfaces to have the required unit. We did this by dividing the heat equation by the thickness of the wall and inputting that thickness into the Wall Thickness entry box. For thin walls like the glass cover, PE cover, window, absorber, and emitter, the heat equations are divided by the thickness of the material, i.e.,* 3 mm *for the glass,* 6 μm *for the PE cover,* 2 mm *for the window, and* 1 mm *for the absorber and emitter. Whereas for the roof and walls, we used the thickness of its coating, i.e., 0.*2 mm.

- ➢ Solution Methods
  - o Pressure-Velocity Coupling Scheme: SIMPLE
  - o Spatial Discretisation:

- Pressure: PRESTO!
- Momentum: Second Order Upwind
- Turbulent Kinetic Energy: First Order Upwind
- Turbulent Dissipation Rate: First Order Upwind
- Energy: Second Order Upwind
- Discrete Ordinates: First Order Upwind
- Transient Formulation: First Order Implicit

➢ Monitors
o Residual checking:

continuity	1×10^{-6}
x-velocity	1×10^{-6}
y-velocity	1×10^{-6}
energy	1×10^{-6}
k	1×10^{-6}
epsilon	1×10^{-6}
DO-intensity	1×10^{-6}

o Reported parameters for convergence checking
- Glass, absorber, and emitter temperatures
- Indoor air temperature
- Indoor air velocity
- Volume flow rate through each opening

➢ Running simulation
o Time step size: 450 s
o Number of time step: 1344 or until the reported parameters converged

References

[1] M.I. Ahmad, H. Jarimi, S. Riffat, Nocturnal Cooling Technology for Building Applications, Springer, Singapore, 2019.
[2] A. Argiriou, Radiative cooling, in: D.A. Matheos Santamouris (Ed.), Passive Cooling of Buildings, Earthscan, New York, 2013, pp. 424–454.
[3] Suhendri, M. Hu, Y. Su, J. Darkwa, S. Riffat, Implementation of passive radiative cooling technology in buildings: a review, Build 10 (2020).
[4] L. Chen, K. Zhang, M. Ma, S. Tang, F. Li, X. Niu, Sub-ambient radiative cooling and its application in buildings, Build. Simulat. (2020), https://doi.org/10.1007/s12273-020-0646-x.
[5] J. Chen, L. Lu, Q. Gong, W.Y. Lau, K.H. Cheung, Techno-economic and environmental performance assessment of radiative sky cooling-based super-cool roof applications in China, Energy Convers. Manag. 245 (2021), 114621, https://doi.org/10.1016/j.enconman.2021.114621.
[6] J. Feng, M. Saliari, K. Gao, M. Santamouris, On the cooling energy conservation potential of super cool roofs, Energy Build. 264 (2022), 112076, https://doi.org/10.1016/j.enbuild.2022.112076.
[7] L. Liu, H. Zhang, Y. Cai, Y. Li, J. Qin, Z. Yang, W. Zhang, C. Feng, Q. Gao, Solar energy materials and solar cells super-amphiphobic coatings with sub-ambient daytime radiative cooling — Part 2 : cooling effect under real conditions, Solar Energy Mater. Solar Cells 241 (2022) 1–9.
[8] T. Hu, T.H. Kwan, G. Pei, An all-day cooling system that combines solar absorption chiller and radiative cooling, Renew. Energy 186 (2022) 831–844, https://doi.org/10.1016/j.renene.2022.01.058.
[9] F. Chi, Y. Liu, J. Yan, Integration of radiative-based air temperature regulating system into residential building for energy saving, Appl. Energy 301 (2021), 117426, https://doi.org/10.1016/j.apenergy.2021.117426.
[10] S. Suhendri, M. Hu, Y. Su, J. Darkwa, S. Riffat, Performance evaluation of combined solar chimney and radiative cooling ventilation, Build. Environ. 209 (2022), 108686, https://doi.org/10.1016/j.buildenv.2021.108686.
[11] A. Radwan, T. Katsura, L. Ding, A.A. Serageldin, A.I. EL-Seesy, K. Nagano, Design and thermal analysis of a new multi-segmented mini channel based radiant ceiling cooling panel, J. Build. Eng. 40 (2021), 102330, https://doi.org/10.1016/j.jobe.2021.102330.
[12] M. Ye, A.A. Serageldin, K. Nagano, Numerical optimization of a novel ceiling radiant cooling panel combined with wall attached ventilation system, Case Stud. Therm. Eng. 26 (2021), 101066, https://doi.org/10.1016/j.csite.2021.101066.
[13] A.A. Serageldin, M. Ye, A. Radwan, H. Sato, K. Nagano, Numerical investigation of the thermal performance of a radiant ceiling cooling panel with segmented concave surfaces, J. Build. Eng. 42 (2021), 102450, https://doi.org/10.1016/j.jobe.2021.102450.
[14] L. Li, C. Zhang, X. Xu, J. Yu, F. Wang, W. Gang, J. Wang, Simulation study of a dual-cavity window with gravity-driven cooling mechanism, Build. Simulat. 15 (2022) 1339–1352, https://doi.org/10.1007/s12273-021-0848-x.
[15] T. Kubota, D. Hooi, C. Toe, D.R. Ossen, Field investigation of indoor thermal environments in traditional Chinese shophouses with courtyards in malacca Malaysia , using field measurements and focuses on the cooling effects of courtyards, J. Asian Architect. Build Eng. 13 (2014) 2–9.
[16] C. Feng, P. Yang, H. Liu, M. Mao, Y. Liu, T. Xue, J. Fu, T. Cheng, X. Hu, H.J. Fan, et al., Bilayer porous polymer for efficient passive building cooling, Nano Energy 85 (2021), 105971, https://doi.org/10.1016/j.nanoen.2021.105971.
[17] D.H.W. Li, J.C. Lam, Solar heat gain factors and the implications to building designs in subtropical regions, Energy Build. 32 (2000) 47–55, https://doi.org/10.1016/S0378-7788(99)00035-3.
[18] K.E. Amori, S.W. Mohammed, Experimental and numerical studies of solar chimney for natural ventilation in Iraq, Energy Build. 47 (2012) 450–457.
[19] M.E. Tiji, M. Eisapour, R. Yousefzadeh, M. Azadian, P. Talebizadehsardari, A numerical study of a PCM-based passive solar chimney with a finned absorber, J. Build. Eng. 32 (2020), 101516, https://doi.org/10.1016/j.jobe.2020.101516.
[20] A.A.M. Omara, H.A. Mohammed, I.J. Al Rikabi, M.A. Abuelnour, A.A. A. Abuelnuor, Performance improvement of solar chimneys using phase change materials: a review, Sol. Energy 228 (2021) 68–88, https://doi.org/10.1016/j.solener.2021.09.037.
[21] M. Rabani, V. Kalantar, M. Rabani, Passive cooling performance of a test room equipped with normal and new designed Trombe walls: a numerical approach, Sustain. Energy Technol. Assessments 33 (2019) 69–82, https://doi.org/10.1016/j.seta.2019.03.005.
[22] L. Moosavi, M. Zandi, M. Bidi, E. Behroozizade, I. Kazemi, New design for solar chimney with integrated windcatcher for space cooling and ventilation, Build. Environ. 181 (2020), 106785, https://doi.org/10.1016/j.buildenv.2020.106785.
[23] A.A. Serageldin, A.K. Abdelrahman, S. Ookawara, Parametric study and optimization of a solar chimney passive ventilation system coupled with an earth-to-air heat exchanger, Sustain. Energy Technol. Assessments 30 (2018) 263–278, https://doi.org/10.1016/j.seta.2018.10.010.
[24] K. Taurines, Energy and thermal analysis of an innovative earth-to-air heat exchanger: experimental investigations, Energy Build. 187 (2019) 1–15, https://doi.org/10.1016/j.enbuild.2019.01.037.
[25] T. Long, D. Zheng, W. Li, Y. Li, J. Lu, L. Xie, S. Huang, Numerical investigation of the working mechanisms of solar chimney coupled with earth-to-air heat exchanger (SCEAHE), Sol. Energy 230 (2021) 109–121, https://doi.org/10.1016/j.solener.2021.10.029.
[26] Ansys® Ansys Fluent 2021 R1, Help System, Fluent User's Guide, Getting Started, ANSYS, Inc.
[27] M. Hu, B. Zhao, X. Ao, Y. Su, G. Pei, Parametric analysis and annual performance evaluation of an air-based integrated solar heating and radiative cooling collector, Energy 165 (2018) 811–824, https://doi.org/10.1016/j.energy.2018.09.127.
[28] B. Zhao, M. Hu, X. Ao, X. Huang, X. Ren, G. Pei, Conventional photovoltaic panel for nocturnal radiative cooling and preliminary performance analysis, Energy 175 (2019) 677–686, https://doi.org/10.1016/j.energy.2019.03.106.

[29] B. Zhao, M. Hu, X. Ao, G. Pei, Performance evaluation of daytime radiative cooling under different clear sky conditions, Appl. Therm. Eng. 155 (2019) 660–666, https://doi.org/10.1016/j.applthermaleng.2019.04.028.
[30] J. Kong, J. Niu, C. Lei, A CFD based approach for determining the optimum inclination angle of a roof-top solar chimney for building ventilation, Sol. Energy 198 (2020) 555–569, https://doi.org/10.1016/j.solener.2020.01.017.
[31] M. Hu, B. Zhao, Suhendri, J. Cao, Q. Wang, S. Riffat, Y. Su, G. Pei, Quantitative characterization of the effect of inclination angle on flat-plate radiative cooling performance in buildings, J. Build. Eng. 59 (2022), 105124, https://doi.org/10.1016/j.jobe.2022.105124.
[32] M. Hu, G. Pei, L. Li, R. Zheng, J. Li, J. Ji, Theoretical and experimental study of spectral selectivity surface for both solar heating and radiative cooling, Int. J. Photoenergy 2015 (2015), https://doi.org/10.1155/2015/807875.
[33] Y. Cui, Y. Wang, Q. Huang, S. Wei, Effect of radiation and convection heat transfer on cooling performance of radiative panel, Renew. Energy 99 (2016) 10–17, https://doi.org/10.1016/j.renene.2016.06.025.
[34] Z.D. Chen, P. Bandopadhayay, J. Halldorsson, C. Byrjalsen, P. Heiselberg, Y. Li, An experimental investigation of a solar chimney model with uniform wall heat flux, Build. Environ. 38 (2003) 893–906, https://doi.org/10.1016/S0360-1323(03)00057-X.
[35] S. Lal, Experimental, CFD simulation and parametric studies on modified solar chimney for building ventilation, Appl. Sol. Energy 50 (2014) 37–43, https://doi.org/10.3103/S0003701X14010125.
[36] M.M. Villar-Ramos, E.V. Macias-Melo, K.M. Aguilar-Castro, I. Hernández-Pérez, J. Arce, J. Serrano-Arellano, H.P. Díaz-Hernández, L.M. López-Manrique, Parametric analysis of the thermal behavior of a single-channel solar chimney, Sol. Energy 209 (2020) 602–617, https://doi.org/10.1016/j.solener.2020.08.072.
[37] A.P. Raman, M.A. Anoma, L. Zhu, E. Rephaeli, S. Fan, Passive radiative cooling below ambient air temperature under direct sunlight, Nature 515 (2014) 540–544, https://doi.org/10.1038/nature13883.
[38] F. Bu, D. Yan, G. Tan, H. Sun, J. An, Systematically incorporating spectrum-selective radiative cooling into building performance simulation: numerical integration method and experimental validation, Appl. Energy 312 (2022), 118733, https://doi.org/10.1016/j.apenergy.2022.118733.
[39] B.B. Naghshine, A. Saboonchi, Optimized thin film coatings for passive radiative cooling applications, Opt Commun. 410 (2018) 416–423, https://doi.org/10.1016/j.optcom.2017.10.047.
[40] J. Zhang, J. Yuan, J. Liu, Z. Zhou, J. Sui, J. Xing, J. Zuo, Cover shields for sub-ambient radiative cooling: a literature review, Renew. Sustain. Energy Rev. 143 (2021), 110959, https://doi.org/10.1016/j.rser.2021.110959.
[41] M. Hu, Suhendri, B. Zhao, X. Ao, J. Cao, Q. Wang, S. Riffat, Y. Su, G. Pei, Effect of the spectrally selective features of the cover and emitter combination on radiative cooling performance, Energy Built. Environ. 2 (2021) 251–259, https://doi.org/10.1016/j.enbenv.2020.06.008.
[42] Kuczyński, T.; Staszczuk, A.; Gortych, M.; Stryjski, R. Effect of thermal mass, night ventilation and window shading on summer thermal comfort of buildings in a temperate climate. Build. Environ. 2021, 204, doi:10.1016/j.buildenv.2021.108126.
[43] K. Dharmasastha, D.G.L. Samuel, S.M.S. Nagendra, M.P. Maiya, Impact of indoor heat load and natural ventilation on thermal comfort of radiant cooling system: an experimental study, Energy Built. Environ. (2022), https://doi.org/10.1016/j.enbenv.2022.04.003.
[44] N.K. Bansal, R. Mathur, M.S. Bhandari, Solar chimney for enhanced stack ventilation, Build. Environ. 28 (1993) 373–377, https://doi.org/10.1016/0360-1323(93)90042-2.
[45] M. Maerefat, A.P. Haghighi, Passive cooling of buildings by using integrated earth to air heat exchanger and solar chimney, Renew. Energy 35 (2010) 2316–2324, https://doi.org/10.1016/j.renene.2010.03.003.
[46] J.K. Calautit, P.W. Tien, S. Wei, K. Calautit, B. Hughes, Numerical and experimental investigation of the indoor air quality and thermal comfort performance of a low energy cooling windcatcher with heat pipes and extended surfaces, Renew. Energy 145 (2020) 744–756, https://doi.org/10.1016/j.renene.2019.06.040.
[47] M. Kottek, J. Grieser, C. Beck, B. Rudolf, F. Rubel, World map of the Köppen-Geiger climate classification updated, Meteorol. Z. 15 (2006) 259–263, https://doi.org/10.1127/0941-2948/2006/0130.
[48] Crawley, D.; Lawrie, L. Climate.OneBuilding.Org Available online: climate.onebuilding.org.
[49] A. Oikonomou, F. Bougiatioti, Architectural structure and environmental performance of the traditional buildings in Florina, NW Greece, Build. Environ. 46 (2011) 669–689, https://doi.org/10.1016/j.buildenv.2010.09.012.
[50] S.K. Meerdink, S.J. Hook, D.A. Roberts, E.A. Abbott, The ECOSTRESS spectral library version 1.0, Remote Sens. Environ. 230 (2019), 111196, https://doi.org/10.1016/j.rse.2019.05.015.
[51] Passipedia Internal Heat Gains in Relation to Living Area Available online: passipedia.org.
[52] M.J. Cook, An Evaluation of Computational Fluid Dynamics for Modelling Buoyancy-Driven Displacement Ventilation, 1998.
[53] vol. 15317, ANSYS Inc., USA, 2013, pp. 724–746. ANSYS FLUENT 13 Ansys Fluent Theory Guide.
[54] B.E. Launder, D.B. Spalding, Lectures in Mathematical Models of Turbulence, Academic Press, London, England, 1972.
[55] G. Gan, Impact of computational domain on the prediction of buoyancy-driven ventilation cooling, Build. Environ. 45 (2010) 1173–1183, https://doi.org/10.1016/j.buildenv.2009.10.023.
[56] S. Gilani, H. Montazeri, B. Blocken, CFD simulation of stratified indoor environment in displacement ventilation: validation and sensitivity analysis, Build. Environ. 95 (2016) 299–313, https://doi.org/10.1016/j.buildenv.2015.09.010.
[57] Ansys® Ansys Fluent 2021 R1, Help System, Fluent User's Guide, Solution Mode, ANSYS, Inc.
[58] P. Berdahl, M. Martin, Emissivity of Clear Skies, Sol. Energy 32 (1984) 663–664, https://doi.org/10.1016/0038-092X(84)90144-0.
[59] L. Evangelisti, C. Guattari, F. Asdrubali, On the sky temperature models and their influence on buildings energy performance: a critical review, Energy Build. 183 (2019) 607–625, https://doi.org/10.1016/j.enbuild.2018.11.037.
[60] C. Melchor V, New formula for the equivalent night sky emissivity, Sol. Energy 28 (1982) 489–498.
[61] R. Tang, Y. Etzion, I.A. Meir, Estimates of clear night sky emissivity in the Negev Highlands, Israel, Energy Convers. Manag. 45 (2004) 1831–1843, https://doi.org/10.1016/j.enconman.2003.09.033.
[62] J. Watmuff, W. Charters, D. Proctor, Solar and wind induced external coefficients - solar collectors, Coop. Mediterr. pour l'Energie Sol. 1 (1977) 56.
[63] M. Hu, B. Zhao, X. Ao, N. Chen, J. Cao, Q. Wang, Y. Su, G. Pei, Feasibility research on a double-covered hybrid photo-thermal and radiative sky cooling module, Sol. Energy 197 (2020) 332–343, https://doi.org/10.1016/j.solener.2020.01.022.
[64] H. Bahaidarah, A. Subhan, P. Gandhidasan, S. Rehman, Performance evaluation of a PV (photovoltaic) module by back surface water cooling for hot climatic conditions, Energy 59 (2013) 445–453, https://doi.org/10.1016/j.energy.2013.07.050.